CORRELATION BETWEEN EQUATORIAL ELECTROJET AND THE OCCURRENCE OF EQUATORIAL IONISATION ANOMALY OVER THE EAST AFRICAN REGION DURING THE SOLAR MINIMUM PERIOD 2008-2009

BY

MILIMU ANEKHA HANNINGTON

A THESIS SUBMITTED IN PARTIAL FULFILLMENT OF REQUIREMENTS FOR THE DEGREE OF MASTER OF SCIENCE IN PHYSICS

SCHOOL OF PHYSICAL AND BIOLOGICAL SCIENCES

MASENO UNIVERSITY

DECLARATION

This thesis is my own work and has not been presented to any University for the award of any degree. Where other peoples' work has been sought, this has been properly acknowledged and referenced in accordance with the Maseno University requirements.

Signature: ..... Date: .....

MILIMU ANEKHA HANNINGTON

MSC/SC/00052/2019

This thesis has been presented with our approval as supervisors.

Signature: ..... Date: .....

Dr. George E. Omondi,
Department of Physics and Materials Science,
Maseno University,
P.O. Box 333-40105,
Maseno-Kenya.

Signature: ..... Date: .....

Dr. Patrick Mungufeni,
Department of Physics,
Muni University,
P.O. Box 725,
Arua- Uganda.

ACKNOWLEDGEMENT

I would like to recognize the presence of the Almighty God in my life and the strength he has given me throughout the time of my studies. In a special way, I would like to express my many thanks to my supervisors; Dr. Omondi George and Dr. Mungufeni Patrick, who introduced me to the field of Space Physics and for the constant support they provided throughout my research period. Many thanks to the Milimu family led by my lovely supportive father Alex Milimu, and my caring mother Mrs. Carolyn Milimu, for always pushing me forward even when the research was challenging. Finally, special thanks to my lovely wife and the mother of my two children Annah, our lovely daughter, Ashley, and lovely son, Adriel for understanding and supporting me throughout the research period.

DEDICATION

To my parents, wife Annah, daughter Ashley, and son Adriel

ABSTRACT

In the electron density distribution at the low-latitude ionosphere, equatorial electrodynamics plays a critical role such as forecasting the dynamics and fluctuations of ionospheric plasma densities. The equatorial electrojet (EEJ) and the equatorial ionization anomaly (EIA) are two major phenomena of equatorial electrodynamics. Studies have been carried out on the strength of EEJ as well as the EIA. However, the following gaps still exist: most studies have been done in Indian and American regions during maximum solar years; yet ionospheric dynamics have a dependence on the longitude; correlations have also not been done during both geomagnetically quiet and disturbed conditions. The correlation between EEJ and EIA was required since EEJ is one of the systems that lift plasma in equatorial regions, causing Equatorial Ionization Anomaly, which suggests a connection between EEJ and EIA. Since it is necessary to get a complete picture during both geomagnetically quiet and disturbed conditions, therefore, the problem of the study is that strong scintillations affect communication and navigation systems. Thus, there is a need to investigate the relationship between EEJ and EIA since they are important for ionospheric space weather and also this will help the development of models that can be used to forecast or nowcast scintillations. Based on the aforesaid knowledge gap the problem of this study is on EEJ's impact on the development of the EIA during the low solar activity period over the East African region. Based on this problem the objectives of the study were (i) To determine the strength of EEJ, (ii) To quantify the strength of EIA and (iii) To analyze the correlation between EEJ and EIA. This study used a pair of International Real-time Magnetic Observatory Network (INTERMAGNET) magnetometers located in Addis Ababa (geographic 9.05°N, 38.76°E, geomagnetic 0.16°N, 110.45°E), the African Meridian B-field Education and Research (AMBER) station in Adigrat (geographic 14.26°N, 39.45°E, geomagnetic 6.1°N, 111.04°E) both in Ethiopia and the total electron content (TEC) derived from a set of International Global Navigation Satellite System (GNSS) signals (IGS) receivers within the East African region. The data used during this period was for both geomagnetically disturbed and quiet conditions. The difference in the horizontal component of the geomagnetic field seen by two ground-based magnetometers was used to estimate the EEJ strength. In determining the EIA strength over the region, TEC over the crest to that above the trough was determined to be in a certain ratio. The peak value of EEJ is 110nT and it occurs between 10:00 and 14:00 LT for geomagnetically quiet conditions. This is due to the high rate of photoionization during this period. These variations in the amplitude of EEJ with time and months is attributed to the monthly movement of the Sq foci northward and equatorward in a given year. The EIA's peak during geomagnetically quiet days is 1.45 and it was recorded between 20:00 – 22:00LT while the peak of EIA during geomagnetically disturbed days is 1.2 and it occurred at 20:00LT. The correlation coefficients were found to vary from moderate to strongest during geomagnetically quiet conditions, ranging from 0.58 to 0.74. During geomagnetically disturbed conditions, the correlation coefficient ranges from 0.28 to 0.45. The significant linear link between EEJ and EIA is caused by the independent increase in the eastward electric field and photo-ionization on TEC. Most panels showed that the ratio of Crest (CT) to trough (TEC) > 1. This research presents patterns in the EEJ and EIA strength over East Africa during the solar minimum period. Since EEJ and EIA influences the occurrence of ionospheric irregularities which in turn lead to scintillations of communication and navigation signals, we recommend simultaneous analysis of EEJ, EIA and scintillation data. This would reveal the influence of EEJ and EIA on the occurrence of scintillations.

TABLE OF CONTENTS

LIST OF ACRONYMS AND ABBREVIATIONS

CMEs	Coronal Mass Ejections
CC	correlation coefficients
EEJ	Equatorial Electrojet
EIA	Equatorial Ionisation Anomaly
ESF	Equatorial Spread F
GNSS	Global Navigation Satellite Systems
H	Horizontal magnetic field intensity
HF	High frequency
IGS	International GNSS Service
IS	IonoSonde
INTERMAGNET	International Real-time Magnetic Observatory Network
LT	Local time
MAGDAS	MAGnetic Data Acquisition System

NNSS	Navy Navigation Satellite System
PPEF	Prompt Penetration Electric Field
PRE	pre-reversal enhancement
RINEX	Receiver INdependent EXchange
SENW	Storm-time Equatorward Neutral Winds
Sq-current	Solar quiet current
TEC	Total Electron Content
TECU	TEC-units
UIDs	Unexpected Ionospheric Disturbances

LIST OF TABLES

LIST OF FIGURES

CHAPTER ONE: INTRODUCTION

This chapter addresses the theoretical elements that guide this thesis. It begins with a brief overview of the Equatorial Electrojet and Equatorial Ionization Anomaly, which are the two most important features of the equatorial and low-latitude ionospheres. The problem statement, study objectives, research questions, study justification, scope, and hypotheses are all presented.

1.1: Background

The E region Sq-current (solar quiet current) system is caused by the global solar-driven wind flowing across the magnetic field lines, resulting in an intensified eastward electric field in the dayside ionosphere. At the magnetic equator within the African region where the geomagnetic field is nearly horizontal, the Sq current systems of the southern and northern hemispheres merge and intensify to form a jet-like current in the E-region of the ionosphere, which is called the "equatorial electrojet" (Venkatesh, Fagundes, Prasad, Denardini, De Abreu, et al., 2015). Equatorial Electrojet (EEJ) is a narrow band of enhanced eastward current flowing in the E-region (100-120km) altitude within ±2° at the geomagnetic equator (Chakraborty & Hajra, 2009a); (Jose et al., 2011a). The incidence of solar radiation is nearly perpendicular in the equatorial regions especially in the equinox month thereby enhancing the effective conductivity of the current. The EEJ is current powered by the tidal winds through the dynamo system that causes the accumulation of positive charges at dawn and negative at dusk terminators.

The secondary polarization electric field (Esz) is created by space charge dispersion and is vertical from the ionosphere's bottom to its top (see Figure 1.1). This secondary polarized electric field induces a vertical Pedersen current that entirely cancels out the Hall current, resulting in an

equilibrium state with no current flowing vertically. This is depicted on the top and bottom of Figure 1.1 with $\sigma_H = \sigma_p = 0$

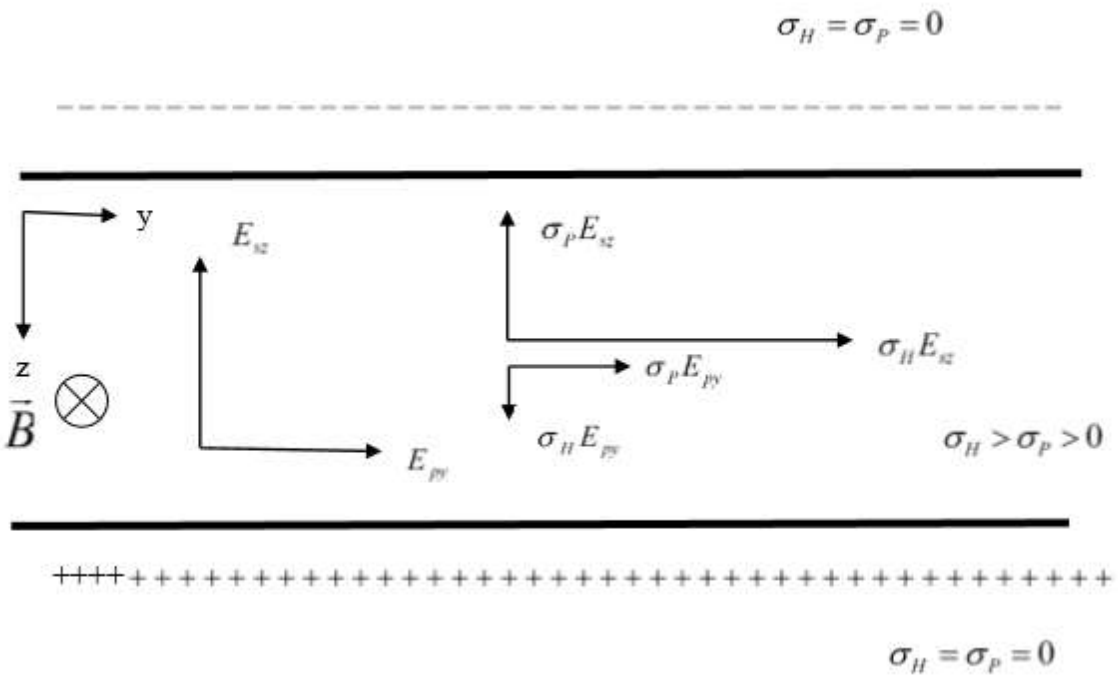

Figure 1.1: Effective conductivities at the geomagnetic equator

Such condition is given by;

$$J_z = \sigma_H E_{py} + \sigma_p E_{sz} = 0 \qquad 1.1$$

where σ_H stands for the Hall conductivity and σ_p, the Pedersen conductivity.

This yields the secondary polarized electric field as;

$$E_{sz} = -\frac{\sigma_H}{\sigma_p} E_{py} \qquad 1.2$$

Besides, a secondary Hall current component (a current flowing in the y-direction orthogonal to both the secondary polarization electric field and the magnetic field directions) is also generated

by the secondary polarization electric field component. The actual Hall current path is the same as the cross product of the secondary polarization electric field (which works in the negative of the specified z-axis) and the magnetic field; thus, the secondary Hall conductivity is defined as;

$$\overrightarrow{J_{sy}} = \sigma_H E_{sz}(-\hat{y}) \qquad 1.3a$$

where $\hat{y}$ is a positive y-directed unit vector.

The Hall conductivity provided in equation (1.3a) can be expressed simply as;

$$\overrightarrow{J_{sy}} = -\sigma_H E_{sz} \qquad 1.3b$$

Substituting equation (1.2) into (1.3b),

$$\overrightarrow{J_{sy}} = \sigma_H [\frac{\sigma_H}{\sigma_p}] E_{py} \qquad 1.4$$

Equation (1.4) can be simplified to;

$$J_{sy} = \frac{\sigma_H^2}{\sigma_P} E_{py} \qquad 1.5$$

The total current flowing eastward (in the positive y-direction) comprises both the Pedersen current, J_{py} , and the secondary Hall current, J_{sy} (see equation 1.6).

$$J_y = J_{py} + J_{sy} = [\sigma_p + \frac{\sigma_H^2}{\sigma_P}] E_{py} \qquad 1.6$$

The Cowling conductivity can be identified from equation (1.6) as;

$$\sigma_c = [\sigma_p + \frac{\sigma_H^2}{\sigma_p}] \qquad 1.7$$

The Cowling conductivity, which is several orders of magnitude more than the usual Pedersen conductivity for normal Hall-to-Pedersen ratios ranging from 3 to 4, explains the intensification and concentration of the equatorial electrojet above the geomagnetic equator. However, across a

stretch of roughly 600 km throughout the dip equator, the terrestrial magnetic field reduces due to the high horizontal jet current, which enhances the magnetic field closer to the dip equator. At the magnetic equator, enhancement fields typically range from 50 to 100 nT around noon.

The conductivity that runs parallel to electric field **E** is known as the Pedersen conductivity. The Hall conductivity is the conductivity perpendicular to both geomagnetic field B_o and E. Joule heating results from the flow of Pedersen currents, which also causes Ohmic losses. The element parallel to $\mathbf{B}_o$ continues to rise with altitude. A west-east oriented electric field around the geomagnetic dip equator produces vertical Hall currents that cannot close resulting in the electric field around the magnetic equator towards the east. The currents of Pedersen and Hall move to the east and downward, respectively, as a result of the crossing fields between northern magnetic and electric fields (Chen et al., 2016). In relation to the high Pedersen conductivity, the Pedersen current flows dominantly at about 130km altitude. Figure 1.1 shows how these conductivities are formed at the geomagnetic equator.

The Equatorial Ionization Anomaly (EIA) is another feature of the characteristic and low latitude ionosphere and it also belongs to the outcome of the ion continuity equation, a well-studied phenomenon specific to the low and equatorial latitudes of the ionosphere. The plasma fountains effect, where the plasma is raised to high latitudes by the action of the eastern electric field and the northward pointing horizontally magnetic field, causes the EIA. After raising the plasma, it diffuses downwards along the geomagnetic field lines on each side of the dip equator under the influence of forces of gravity and pressure gradients, and this is illustrated in Figure 1.2. The figure shows the orientation of the East-ward electric field, the north-ward magnetic field, and the diffusion of plasma along the magnetic field lines. As a result, the horizontal dispersion of electron

density throughout the equatorial/low latitude ionosphere, known as the EIA, develops a double hump pattern.

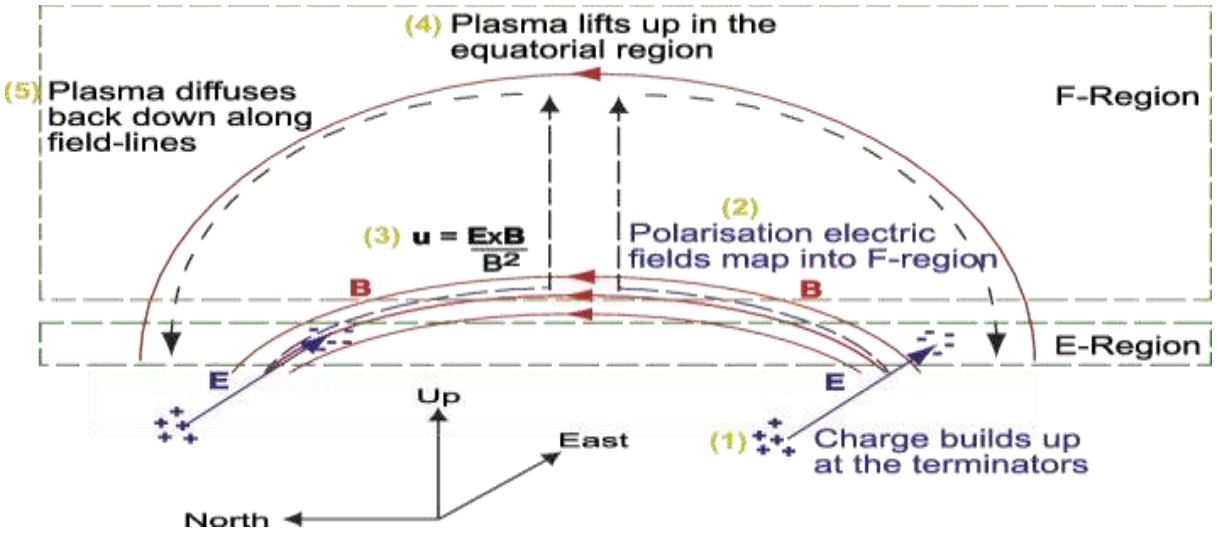

Figure 1.2: Development of the EIA

Diffusion proceeds quickly in the F-region, but even more slowly in the low ionosphere (F_1 region), where based on the continuity equation of ion, the collision between charged and neutral particles prevails (Pedatella et al., 2014; Huang et al., 2014a) This implies that without the transport mechanism, the low ionosphere is defined by the ion generation and loss, while the F region and its top are dominated by all variables of ion continuity equation. Ion density changes in the F region are described by:

$$Q = p - \beta n - \nabla(\phi) \qquad 1.8$$

Equation 1.8 relates the rate of ion concentration, Q, loss coefficient, β, rate of production, p, ion concentration, n, and the rate of drift of ions, ϕ. The last term constitutes the transport impacts as a result of thermospheric meridional neutral winds, electric fields, and ambipolar diffusion. This term mainly reflects the mechanism in charge of initiating EIA plasma hemispheric transport. EIA

can also be described as the plasma redistribution between the hemispheres, resulting in a low latitude peak in each hemisphere and reduced plasma (trough) marginally above the dip equator in each hemisphere (Yamazaki et al., 2014a). It ought to be noted that production and loss variables are both active in the plasma transport through the F-region (Rush et al., 1969).

The radio waves that traverse the ionosphere experience intermittent amplification and fade called scintillations due to ionospheric irregularities caused by intricate physical phenomena in the solar-terrestrial environment. When these scintillations are strong, they affect navigation and communication systems (Abadi et al., 2014). Through low solar activity years, it is assumed that ionospheric conditions are almost constant with respect to time due to geomagnetic storms, weather conditions, Season, solar activity and season. However, during and after a high solar activity period, ionospheric conditions change very rapidly. Throughout the 11 (eleven) year solar sunspot period, the frequency of geomagnetic disturbance varies, becoming more common as sunspot counts increase. The sun undergoes an alternating radiation cycle of around 11 years, called the solar (sunspot) cycle. The ionosphere has a larger electron density when compared to other times during solar maximum periods (most sunspots).

The physical dynamics which necessitate the correlation between EEJ and EIA is that EEJ is one of the systems responsible for the plasma uplift in the equatorial regions thereby generating Equatorial Ionization Anomaly, which indicates a linkage between EEJ and EIA. Therefore, much research has been conducted to understand this linkage.

Research has been done to understand the EEJ's effect on the development of the EIA due to significant changes in electron densities from either side of the magnetic equator. This affects signals of the ionospheric radio frequency and communication systems with the ground-to-ground high-frequency, but since the dynamics of the ionosphere depend on various factors including the

solar cycle, geomagnetic storms , geographical locations and time and also most of the EEJ and EIA studies have been conducted on Indian and American region, this study will focus on the EEJ and EIA correlation in the East African region.

The knowledge gaps identified by this study are that correlations have not been done during geomagnetically disturbed and quiet conditions. It is necessary to get a complete picture of both geomagnetically disturbed and quiet conditions.

The East African sector was chosen as a study region since the studies done over this region are during high solar activity period (Rush et al., 1969; Mungufeni et al., 2018). Therefore, we have limited knowledge of the relation between the EEJ and the development of the EIA in the East African region during the solar minima. This research performed the correlation between EEJ and EIA during the solar minimum years of 2008 and 2009 over the East African region.

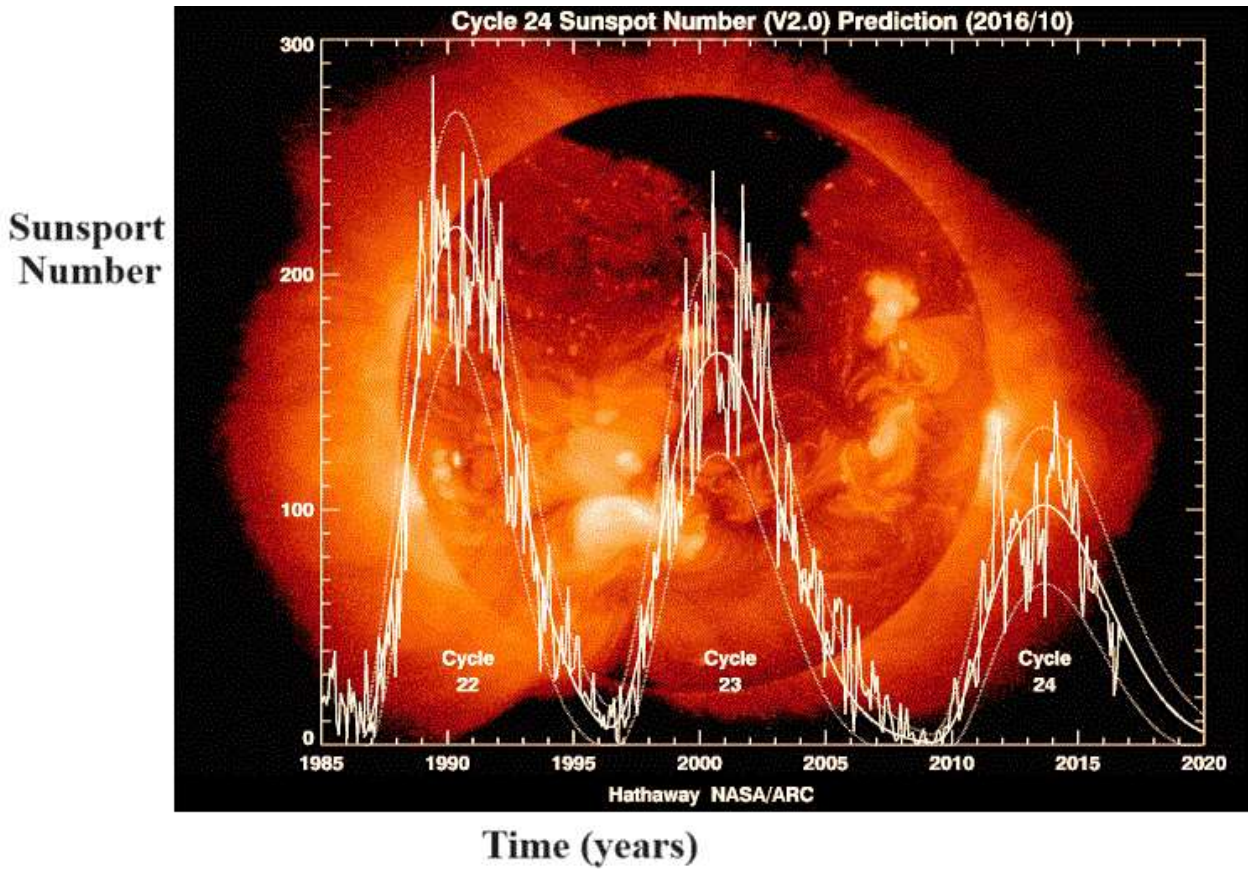

Figure 1.3: Progression of the sunspot cycle.

Moreover, this study compared the results obtained over this region to those in the Indian and American sectors.

1.2: Statement of the problem

Due to significant changes in electron densities on either side of the magnetic equator, affecting ionospheric radio frequency signals and ground-to-ground high-frequency communication systems, research has been done to understand the EEJ's effect on the development of the EIA. The knowledge gaps include a lack of results during the low solar activity period; most studies have been done in Indian and American regions during maximum solar years, yet ionospheric dynamics have a dependence on the longitude; correlations have also not been done during both geomagnetically quiet and disturbed conditions. Based on the aforementioned knowledge gaps,

this study investigated the correlation between EEJ and EIA over the East African region during the solar minimum period in the years 2008 – 2009 with a view to getting a complete picture during both geomagnetically quiet and disturbed conditions.

1.3: Objectives of the study

1.3.1 The general objective of the study

To investigate the strength of EEJ and EIA as well as their correlation during the solar minimum period from the year 2008 to 2009 over the East African region.

1.3.2 Specific objectives

i. To determine the strength of EEJ during the solar minimum period from the year 2008 to 2009 over the East African region.
ii. To quantify the strength of EIA during the solar minimum period from the year 2008 to 2009 over the East African region.
iii. To analyze the correlation between EEJ and EIA during the solar minimum period from the year 2008 to 2009 over the East African region.

1.4: Research questions

i. To what extent would EEJ correlate with the EIA during low solar activity years?
ii. Are the responses of EIA to EEJ over the East African region similar to that of Indian and American regions?

1.5: Justification of the study

The results of this study obtained regarding the investigation of the strength of EEJ and EIA and their correlation will help in the development of models that can be used to forecast or nowcast

ionospheric conditions as well as form the basis for further ionospheric research over the East African region.

1.6: Scope of the study

This study has covered the correlation between EEJ and EIA during the solar minimum period from the year 2008 to 2009 over the East African region.

1.7: Hypotheses

i. There exists a strong positive relation between EEJ and EIA strengths.

ii. The trough is located somewhat South of the magnetic equator since the main EEJ center swings slightly south of the magnetic equator over East Africa.

CHAPTER TWO: LITERATURE REVIEW

This chapter reviews the existing scholarly work relevant to the current study. The chapter has been split into three parts 2.1, 2.2, and 2.3. Subsection 2.1 discusses previous studies on the EEJ, Subsection 2.2 explores research on the strength of EIA, and Subsection 2.3 reviews the literature regarding the link between EEJ and EIA. The available body of information within every sub-topic has been presented chronologically.

2.1: The Equatorial Electrojet (EEJ)

As mentioned in section 1.1, the EEJ is a tiny band of intensified eastward current that flows in the E-region (100-120km) altitude within ±2° at the geomagnetic equator. The EEJ manifests as an abnormally large amplitude of variations in horizontal magnetic field components measured at equatorial geomagnetic observatories. It should be noted that when EEJ changes its direction to the West it is known as the Counter Equatorial Electrojet (CEJ). The E-region dynamo, which is responsible for both vertical plasma drift and the EEJ, mainly controls the daytime electrical field (Sethia et al., 1980a). Additionally, Cowling conductivity influences the strength of EEJ. It was found that (Sethia et al., 1980a) magnetic action has little effect on the EIA strength while it has a greater effect on the EEJ strength.

Jose et al., (2011a) observed a short-lived EIA on the day with CEJ in the afternoon and the lack of the EIA on a day when no Electrojet was formed. They contrasted the height of the F2-layer peak in the Brazilian longitude region to the strength of the EEJ across the same longitude sector for September and October 1986. For both local time and day-to-day variance, they reported a strong positive correlation between the F2-layer height and EEJ strength (Jose et al., 2011b).

Kalita et al., (2016) built an empirical model of the EEJ magnetic signature, including local time and longitudinal dependence, based on concurrent measurements made at 12 magnetometer stations spread across six distinct longitude sectors. They then normalized the observation data to the dip equator. The investigation revealed that between 09:00 and 10:00 LT, the EEJ component was strongest in the South American sector and weakest in the Indian sector, but from 11:00 to 14:00 LT, it shifted to the African sector. In conclusion, the study's improved empirical model was able to accurately predict the global components of the EEJ around midday.

Joshi et al., (2016) did observations on the strength of EEJ in the Peruvian sector using data from ground-based observations with the aim of finding reliable precursors of the occurrence of ionospheric irregularities. They observed that the EEJs are enhanced and centered about local noon time along the magnetic equator. The local noontime EEJ is more intense during equinox months than that in solstice months. It was also noted that the location, strengths, and span of the anomaly crests show a large degree of variability. The occurrence of strong corresponding noontime EEJ leads to well-formed late afternoon anomaly crests.

Using data from 12 magnetometer stations located in six longitude sectors during the year 2009, Rabiu et al., (2017) analyzed the EEJ current peak time at various longitude sectors. They discovered that EEJ is strongest in the South American sector. This is due to the fact that over South America, the difference between the dip latitude and the geographic latitude is the highest.

Their findings indicated that the highest EEJ during solar minimum is seen at 11 LT in the South American, Indian, and Southeast Asian sectors, whereas in the African sector, the EEJ occurred at 10 LT.

Lühr et al., (2021) outline a simple approach to estimating the strength of EEJ using the Magnetic Data Acquisition System (MAGDAS). He observed the daily variation of the geomagnetic field component at the equatorial station which is caused by the superimposition of the Sq current and the EEJ current flowing eastward at a lower altitude.

2.2: The strength of Equatorial Ionization Anomaly (EIA).

Stolle et al., 2008 studied the link between the zonal electric field and the EIA in the Peruvian region and compared the findings to EEJ against EIA strength relationships. They found that the EEJ strength and the zonal electric field were good indicators for EIA intensity. Both studies show excellent correlation values of cc > 0.8.

Mungufeni et al.,2018, Huang et al.,2014 and Chen et al.,2008 proposed that the latitudinal gradient of the EIA between the trough and the crest indicates the strength of the EIA (Mungufeni et al., 2018; Chen et al., 2008a; Huang et al., 2014b).

(Balan et al., 2018) reviewed the EIA and the ionospheric irregularities. It was observed that the EIA develops in the morning, continues to exist well beyond the sunset, and covers up to half the global area in 24 hours. They concluded that during the early stages of the daytime (around noon) main phase of major geomagnetic storms the plasma fountain becomes a super fountain and EIA becomes strong. The strong EIA under magnetically active conditions arises from the simultaneous impulsive action of eastward prompt penetration electric field (PPEF) and storm-time equatorward neutral wind (SENW).

In the quiet days of the year 2013 along longitude 35^{o} E, Amaechi et al., 2020 examined the variability of ionospheric anomalies over the African EIA. Emphasis was given on features including the EIA's contribution, the asymmetry of the irregularities over the crests, and the

anomalies that appeared after sunset and after midnight. Their findings revealed that: (1) The position of the African EIA trough varied between 2.2^{o} S and 3.0^{o} N magnetic latitude; (2) The Equinoctial asymmetry across the African EIA crests and trough relied on the location of the crests with regard to the magnetic equator in both hemispheres and on the magnitude of post-sunset equatorward electric field (EEF).

Habyarimana et al., (2020) presented a study that looked at the ionospheric responses to the total solar eclipse that occurred on July 2nd, 2019 across the South American sector. Their data was gathered using GNSS receivers and ionosonde (IS) radar (Jicamarca). TEC decreased by 35% and increased by 57% in the sub-EIA crest and surrounding the EIA crest, respectively, during eclipse totality at sub-EIA latitudes. Their study implies that the observed considerable TEC boost at the EIA crest was driven by enhanced plasma fountain effects (at the magnetic equator) caused by eclipse-induced vertical drift and the dynamo electric field.

Eastes et al., (2019), empirically demonstrated the EIA crest magnitude and its consequences for nighttime equatorial ionospheric plasma irregularity characteristics. This was done at a dip equatorial station in Trivandrum utilizing GPS - TEC data as well as ionosonde data. Their research shows that the amplitude of the EIA crest in the evening hours has a direct influence on the base height of the postsunset ionospheric F- layer (the principal factor responsible for the development of ionospheric plasma irregularities) on a daily basis. The equatorial spread F anomalies are also observed to manifest earlier (later) and to be sustained for a longer (shorter) duration when there is a strong (weak) EIA crest.

2.3: Correlation between EEJ AND EIA.

Dunford (1967) was the first to use topside sounder data to report a significant correlation betwee n EIA strength and the EEJ at the equatorial station, where he defined the EIA strength as the EIA depth D as in equation 2.1,

$$D = \frac{N_p - N_e}{N_e} \quad , \qquad 2.1$$

where N_p is the electron density at the crest and N_e is the magnetic equator electron density

Equation 2.1 is multiplied by width W given in equation 2.2 to get equation 2.3.

$$W = Lat_p - Lat_e \, , \qquad 2.2$$

where Lat_p and Lat_e are the latitudes of the crest and trough respectively.

$$\left(\frac{N_p - N_e}{N_e}\right) W \qquad 2.3$$

Equation 2.3 gives the strength of the EIA.

The EIA parameters they got between 14:00 and 16:00 LT showed the highest correlation, with a lag of 2-3 h between the two. At the equinoxes and June solstice, the correlation is observed to be at its highest and lowest points respectively. This was attributable to the high electrodynamic regulation through the equinoxial months. Rush and Richmond (1973) investigated the relationship between noon EEJ levels and EIA using foF2 data. They noted a positive correlation (correlation coefficient ranging from 0.52 to 0.67) for EIA strength obtained between 14:00 and 16:00 LT. Deshpande et al., 1977 observed a strong EIA on days with strong EEJ, a slightly short EIA on days with a CEJ in the afternoon, and a lack of the EIA on days with no electrojet. They suggested a response period of 2 to 3 hours for the anomalous crest to changes in E-layer dynamics.

Raghavarao et al.,1978 found a 0.9 connection between the electron density at 500 km altitude and the integrated EEJ strength over time (Raghavarao et al., 1978).

According to (Sethia et al., 1980b), the development of the EIA crest is robust during a strong EEJ day, weak during a CEJ day, and does not form at all on a geomagnetically disturbed day. They used TEC data from the ATS 6 geostationary satellite to demonstrate the seasonal changes of the EIA (summer, winter, and equinox). They discovered a strong link between the peak EIA strength and the peak value of the horizontal magnetic field for all seasons. A consistent time difference between the highest EIA and the EEJ current of 3-4 h was also recorded, which was considered to be the time needed for the EIA's evolution (Sethia et al., 1980b).

Using TEC data from the ATS 6 geostationary satellite, Balan et al., (2009) determined the seasonal variation of the EIA with regard to the EEJ strength (summer, winter, and equinox). For all seasons, they discovered a strong link between the peak EIA strength and the peak value of the horizontal magnetic field. They also observed a continuous time gap of 3-4 h between the maximum EIA and the EEJ current, which was interpreted as the time required for the EIA to evolve. A further increase in the relations between EEJ and EIA was observed by Rastogi and Klobuchar, 1990 when average EEJ strength was used ranging from 07:00 to 14:00 LT (Rastogi & Klobuchar, 1990).

Chen et al., (2008) reported the EEJ strength in the Asian sector to be similar to those shifts in the horizontal electric field strength near the magnetic equator to the east. Consequently, in the distribution of electron density across the ionosphere equatorial and low latitudes, the eastward electric field plays a critical role.

Stolle et al., (2008) used satellite observations to show that the EIA ratio of Crest to Trough responds to fluctuations in vertical drift values with a time delay of 1-2 h and EEJ strength of 2-4

h. On geomagnetically quiet days over the Indian subcontinent, the time delay between the EIA and EEJ is often 2-4 hours (Stolle et al., 2008).

Huang et al., (2014b) calculated the latitude of the EIA crest using data from the Navy Navigation Satellite System (NNSS) and the ETS-2 satellite. Abadi et al. (2014) discovered a strong link between the height of the F2 peak layer in the trough region and the EEJ strength in the Brazilian region. They also discovered a response time of 2.5-4 h between the height of the F2 peak above the equator and enhanced electron density at the EIA crest. The response time was proposed to be dependent on the vertical drift velocity and the height of the F2 layer.

(Venkatesh, Fagundes, Prasad, Denardini, de Abreu, et al., 2015) studied the role of the EEJ in the EIA using TEC data from the Indian and American sectors, finding that periodic changes in the strength of the EEJ are significant in the creation and growth of the EIA. The discovery of twin peaks was one of their most notable discoveries. The above literature provides knowledge of EEJ strength-driven EIA.

As noted here, a number of correlation studies have been presented so far between the EEJ and the EIA, but to our knowledge, there is no paper that also statistically examines the relationship between the EEJ and the EIA in the East African region during the low solar activity period for both geomagnetically quiet and geomagnetically disturbed conditions. This study investigated the EEJ and the occurrence of the EIA during the low solar cycle of the years 2008 and 2009 over the East African region to get a complete picture of both geomagnetically quiet and disturbed conditions. This will help the development of models that can be used to forecast or nowcast scintillations as stated in the significance of the study. This can be done by answering the following issues: to what degree is the electric field associated with the EIA? Are these outcomes different from EEJ strength correlations? Addressing these problems will provide new insights into the

usefulness of the EEJ's strength as a proxy for the strength of the EIA. As mentioned earlier this study chose the period of study from 2008 to 2009 since it is a low solar activity period whose electrodynamic processes differ from those of high solar activity periods.

In this work, the TEC derived data from a set of International Global Navigation Satellite System (GNSS) Service (IGS) receivers around the East African region was used to study the EEJ and EIA during the solar minimum years of 2008 and 2009 over the region.

A recent study by Lühr et al., (2021) revealed that the relationship between the EEJ strength and the EIA crest location is distinctly different in the eastern Asian and American sectors, which implies that the EEJ, EIA correlation in Eastern Africa may also exhibit longitudinal variations.

CHAPTER THREE

DATA AND METHODS

The current chapter provides information on the study area and the sets of data in section 3.1 and the methodology used in section 3.2. The detailed procedures to accomplish the stated objectives and ultimately answer the research questions are discussed in sub-sections 3.2.1 (Determination of the EEJ strength), 3.2.2 (Quantification of the strength of EIA), and 3.2.3 (The investigation of the link between EIA and EEJ).

3.1: Data and region of study

In this study, the data used were obtained from the East African longitude region bounded by geographic 30 - 45°E longitude and 12 - 15°N latitude. The sites of the magnetometers at Adigrat (ETHI) are listed at *http://www.magnetometers.bc.edu* and Addis Ababa (AAE) (geographic 9.04°N, 38.77°E, geomagnetic 0.17°N, 110.47°E) (*http://www.intermagnet.org*) both in Ethiopia that were employed in this study to investigate the EEJ's strengths are displayed in Figure 3.1 by blue stars. The red stars in the figure represent the Global Positioning System (GPS) stations.

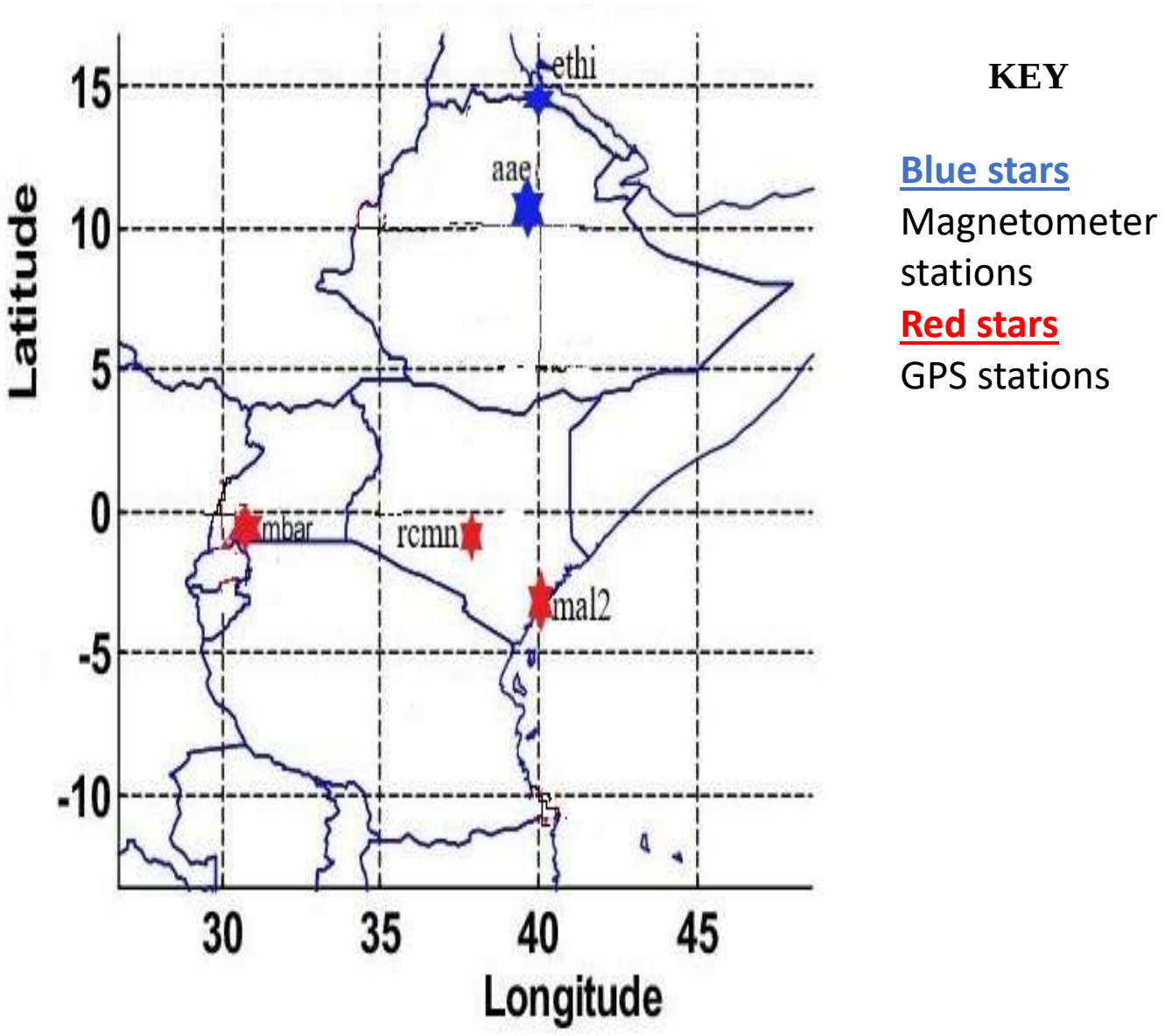

Figure 3.1: A map of GPS receiver and magnetometer sites used in this study

The list of station names, their codes, and geographical and geomagnetic coordinates used in this research are shown in Table 3.1.

Table 3.1: Table showing the magnetometer and GPS receiver stations used in this study

S/N	Station name/Country	Station codes	Geographic Lat. (°)	Geographic Lon. (°)	Geomagnetic Lat. (°)	Geomagnetic Lon. (°)
1.	Addis Ababa (Ethiopia)	AAE	8.97	38.75	0.17	110.48
2.	Adigrat (Ethiopia)	ETHI	14.28	39.46	6.0	111.06
3.	Nairobi (Kenya)	RCMN	-1.24	36.81	10.76	108.51
4.	Malindi, Kenya	MAL2	-3.1	40.1	-12.4	10.5
5.	Mbarara, Uganda	MBAR	-1.23	32.4	10.32	17.3

The Kp-index, Disturbance storm time (Dst)-index, and Auroral electrojet (AE) index are commonly used geomagnetic activity indices. A brief description of these indices is given in subsections 3.1.1, 3.1.2, and 3.1.3, respectively.

3.1.1: The Kp- index

The Kp index is used to indicate the severity of the global magnetic disturbances in near-Earth space**.** There are 28 discrete steps between the values of 0 (very calm) and 9 (extremely disturbed), giving values of 0, 0+, 1-, 1, 1+, 2-, 2, 2+,..., 9. Usually, a level of $K_p \leq 2+$ is chosen as a quietness level while that of Kp ≥ 5+ is the disturbed one (Campbell, 2003) .

3.1.2: The Dst index

Equatorial ring current causes variations in the geomagnetic field, which are quantified by the Dst index. It is calculated from the H-component at hourly intervals at about four stations close to the equator (Omondi et al., 2017). The value of the minimum Dst is frequently used as a measure for classifying the strength of geomagnetic storms. For instance, Loewe and Prolss (1997) divided electric field strength into four categories: weak (-30nT), moderate (-50nT), strong (-100nT), severe (-200nT), and enormous (-350nT).

3.1.3: Auroral electrojet (AE)

AE index is designed to provide a global quantitative measure of auroral zone magnetic activity produced by enhanced ionospheric currents flowing below and within the auroral oval (Raghavarao et al., 1978). It is the total range of deviation at an instant of time from quiet day values of the horizontal magnetic field (H) around the auroral oval (Amaechi et al., 2018).

In the present study, the Kp index was used since it is global. It is also related to the peak-to-peak fluctuations of the horizontal magnetic field component observed on a magnetometer during a three-hour interval relative to a quiet day.

Another set of data used in this study is the Total Electron Content (TEC) data described in subsection 3.1.4.

3.1.4: Total Electron Content Data

The GNSS data that was saved in RINEX files, or Receiver INdependent EXchange files, were used in this study. The information was obtained from the University NAVstar Consortium (UNAVCO) website at *http://www.unavco.org/pub/rinex*. Data obtained from GNSS receivers across the 31°- 41° Longitude sector of Africa was used to calculate the strength of the EIA, the

Longitude is restricted in order to ensure that all the stations have the same local time and that the electrodynamics of the ionosphere is the same in all the stations. The stations under consideration have a limited latitudinal range that is often south of the dip equator. However, a few stations well north of the dip equator were taken into account in order to pinpoint the EIA trough across the region. Both geomagnetically quiet days (Kp≤2+) and geomagnetically storm days data (Kp≥5+) were put into consideration.

3.2: Methodology

3.2.1: Estimation of the Equatorial Electrojet (EEJ) strength.

The difference between the horizontal component (H) of the earth's magnetic field's magnitudes measured by magnetometers at ETHI (H_{SE}) and those estimated at AAE (H_{SA}) for the same days was used to determine the EEJ strength (Srinivasu et al., 2019). An indirect measure of the daytime electrojet current is the difference observed between the two horizontal components (Delta H) (Mungufeni et al., 2018).

To compute the horizontal component, the elements used to describe the earth's magnetic field displayed in Figure 3.2 were considered.

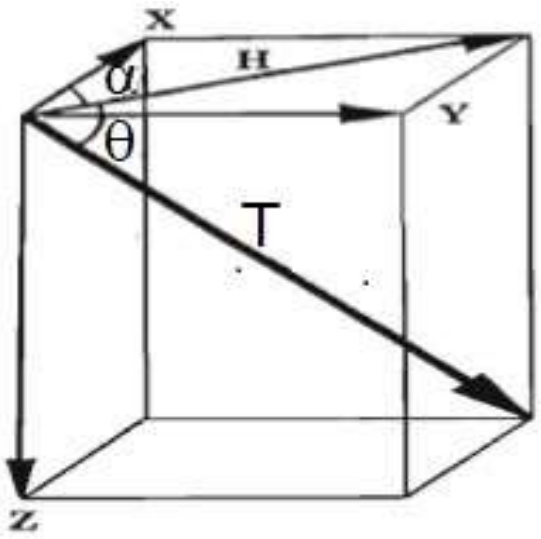

Figure 3.2: Geomagnetic field elements

The angle of depression (θ), is the angle between the true north and the magnetic north, The angle α is used to indicate how steeply the field is tilted with respect to the horizontal (see Figure 3.2). The vectors **H, Z,** and **T** are used to describe the field's intensity. The horizontal intensity, **H** is used to define the horizontal component of the total magnetic field whereas **Z** defines the vertical component. **T** is the sum of the magnetic field strength.

Northerly intensity (X) and easterly intensity (Y) are further divisions of the horizontal field components. The relationship between these components is shown in equations 3.2a, 3.2b, 3.2c, and 3.2d

$\cos\theta = \frac{X}{H}$, this implies that $X = H\cos\theta$ 3.2a

$\sin\theta = \frac{Y}{H}$, this implies that $Y = H\sin\theta$ 3.2b

Using Pythagoras' theorem,

$$X^2 + Y^2 = H^2(\sin^2\theta + \cos^2\theta) \quad 3.2c$$

Using the trigonometric identity, $\sin^2\theta + \cos^2\theta = 1$, the right-hand side of equation 3.2c reduces to H^2 , thus;

$$H = (X^2 + Y^2)^{\frac{1}{2}} \quad 3.2d$$

The H-component, for each day from both ADIS and ETHI data, was obtained using equation (3.2d).

Since magnetospheric currents have an impact on both ADIS and ETHI during the entire month, the baseline was therefore important to effectively eliminate the contributions of magnetospheric currents. The horizontal magnetic field was recorded 150 minutes before and after midnight on each day, and its arithmetic mean served as the baseline. The 300 minutes flanking local midnight was chosen as a baseline since it is now very constant.

$$H_B = \frac{1}{300}\sum_{t=1}^{300} H_t \quad 3.2e$$

To account for various offset values of different magnetometers, the baseline value (H_B) of each day was subtracted from each of the one-minute resolution H-field values according to equation

3.2f (Yamazaki et al., 2014b). The values that were obtained after subtracting H_B from H for a specific station were denoted as H_S.

$$H_s = H - H_B \qquad 3.2f$$

To get the EEJ, the H_S values recorded at ETHI (H_{SE})were then subtracted from those of the corresponding days computed at AAE (H_{SA}) in accordance with equation 3.2g below.

$$EEJ = H_{SA} - H_{SE} \qquad 3.2g$$

The results obtained using equation 3.2g can be found in Figures 4.1, 4.2, 4.3, 4.4, 4.5 and 4.6.

3.2.2: Quantifying Equatorial Ionization Anomaly strength.

The TEC is defined as the total number of electrons integrated along the path from the receiver (R) to the GPS satellites (S), mathematically written as,

$$\mathrm{TEC} = \int_R^S N_e\,(\mathrm{P_i})\mathrm{d}s_i \qquad 3.2h$$

where N_e is the accumulated number of electrons in each square metre through the differential distance ($\mathrm{d}s_i$) along the path from the satellite to the ground-based receiver, p_i.

The TEC is a parameter used to describe the ionosphere, usually expressed in TEC units (TECU) with 10^{16} electrons per square meter equivalent to 1 TECU.

It can be determined from the phase delay or advance of GPS signals when they pass through the ionosphere. The nominal range is 10^{16} to 10^{19} electrons per square metre with minima and maxima occurring at night and the day, respectively. At night the TEC decays rather slowly due to the recombination of electrons and ions.

The Receiver INdependent EXchange (RINEX) observation files were downloaded from the MAL2, MBAR, and RCMN, IGS from 1st January 2008 to 31st December 2009.

The software developed by Gopi Seemala was used to carry out a calibration in order to obtain the intended (CMN) output files. Data for all observable satellites and elevation angles are available in the CMN files. In order to exclude the impacts of multipath, only the data from satellites with elevation angles greater than 30 were used.

The data were analyzed as follows: The daily VTEC data were classified into months for all the days throughout the study period. As a result, 12 monthly bins were created for each year from the years 2008 to 2009 data. The monthly bins were classified further according to local time. This yielded the March equinox (January, February and March) June solstice (April, May and June), September equinox (July, August and September) and December solstice (October, November and December). The monthly average TEC with 30s resolution was calculated using the mean values of the LT bins. The ratio of TEC recorded at the peak to that measured at the trough was calculated to establish the EIA strengths (CREST:TROUGH ratio). The benefit of the CREST:TROUGH ratio over other approaches (Calculating the difference between the TEC obtained at the peak and that measured at the trough, estimating the normalized difference between the TEC measured at the crest and that measured at the trough, and using the TEC measured at the crest's peak) is that it offers a relative variation of the EIA, which is typically effective at illustrating variation in physical phenomena (Yue et al., 2014).

To quantify the EIA the TEC values at the crest were divided by those at the trough, yielding the crest-to-trough TEC ratio. The results obtained are presented in Figures 4.7, 4.8, 4.9, 4.10, 4.11, 4.12 and 4.13.

3.2.3: Analyzing the link between EEJ and EIA

Correlation is a quantitative measure that indicates the extent to which two or more data sets fluctuate in relation to each other. On the other hand, a statistical measure of the strength of the linear relationship between two variables is the correlation coefficient. There are different types of correlation coefficients. In this study, Pearson's correlation coefficient was used since it allows for strong inferences. It is also parametric and measures linear relationships. This means it gives information about the magnitude of the correlation, as well as the direction of the relationship.

The correlation coefficient is obtained using the formula:

$$r = \frac{\sum(x_i - \bar{x})\,(y_i - \bar{y})}{\sqrt{\sum(x_i - \bar{x})^2\ \sum(y_i - \bar{y})^2}} \qquad 3.3$$

where r is the correlation coefficient, x_i represents the values of the x- variable in a sample, $\bar{x}$ is the mean of the values of the x-variable while y_i and $\bar{y}$ are the values of the y-variable in a sample and the mean values of the y-variable respectively.

The correlation between EEJ and EIA was required since EEJ is one of the systems that lift plasma in equatorial regions, causing Equatorial Ionization Anomaly, which suggests a connection between EEJ and EIA. As a result, extensive research has been done to comprehend this connection.

The scatter plots of EEJ against EIA were made and the statistical parameter like correlation coefficient (r) value associated with these data was determined. The results for this correlation are found in Figures 4.14, 4.15, 4.16 and 4.17.

CHAPTER FOUR

RESULTS AND DISCUSSION

The detailed results of the study are presented in this chapter. Section 4.1 presents the EEJ strength while the EIA strength and its connection with the EEJ are presented in sections 4.2 and 4.3 respectively, for the region of East Africa. The findings obtained are discussed, explanations and comparisons to other studies have also been provided in sub-sections 4.1.1, 4.1.2, 4.2.1**,** and 4.2.2 namely, the EEJ on Geomagnetically Quiet Days, the storm perturbation on EEJ during Geomagnetically Disturbed Days, the EIA on Geomagnetically Quiet Days and the EIA on Geomagnetically Disturbed Days respectively.

4.1: The Equatorial Electrojet (EEJ) strength over the East African region.

4.1.1 The EEJ on Geomagnetically Quiet Days

The EEJ for the quiet days during the study period was calculated using equation (3.2f). The results are presented in Figures 4.1 and 4.2, panels (a) – (l). Figures 4.1 and 4.2 present the average EEJ for the selected most quiet days from January - December 2008 and 2009, respectively. The data presented in Figure 4.1 are for geomagnetically quiet days for the year 2008 while Figure 4.2 presents the geomagnetically quiet days for the year 2009. From both panels in Figures 4.1 and 4.2, it is seen that the peak value of EEJ which ranges from 50 - 110nT occurs between 10:00 LT and 14:00 LT. This is attributed to the highest rate of photoionization during this period.

Figure 4.1 reveals that the highest peak of EEJ occurred in August 2008 recording 110nT while panels (g) and (i) show the lowest peak of EEJ (48nT) which was in July and September 2008.

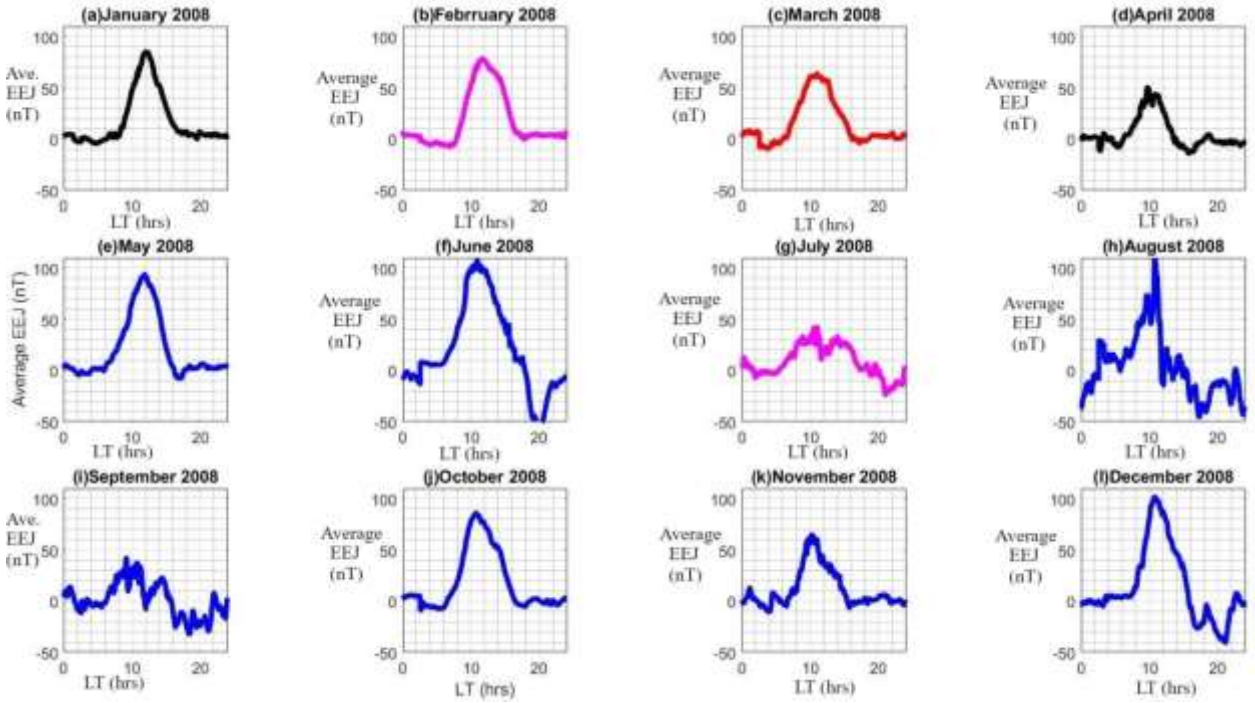

Figure 4.1: Average EEJ against local time during geomagnetically quiet days in 2008

During the year 2009, the highest peak of 96 nT can be seen in November 2009 while July and September 2009 show the lowest peak (see panels (g), (k) and (i) in Figure 4.2).

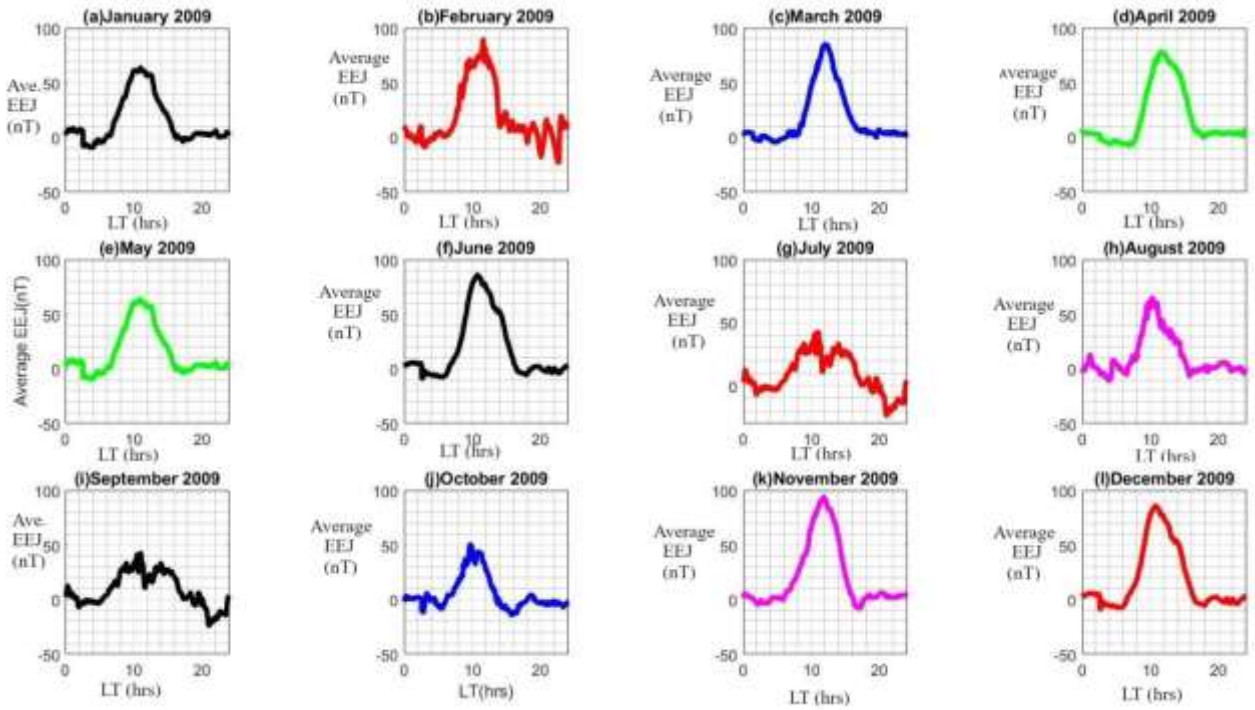

Figure 4.2: Average EEJ against local time during geomagnetically quiet days in 2009

The monthly fluctuations in the timing of the maximum EEJ in Figure 4.1 reveal that the peak in the March equinox (January, February and March) occurs later (~12:00 LT noon) compared to other months (>10:00 LT). These variations in the amplitude of EEJ with time and months can be attributed to the monthly movement of the Sq foci northward and equatorward in a given year.

4.1.2: The Storm perturbation on EEJ current during Geomagnetically Disturbed Days

The geomagnetically disturbed days of 9th March, 21st June, 22nd September 2008 and 22nd July 2009 when the Kp – index was ≥ 5 were considered. The storm perturbation on EEJ during geomagnetically disturbed days was determined and the results are presented in Figures 4.3, 4.4, 4.5 and 4.6. As in Figures 4.1 and 4.2, the storm perturbation on EEJ peak in Figures 4.3, 4.4 and 4.5 also occurs between 10:00 and 14:00 LT. The storm perturbation on EEJ's maximum value occurs at 10:00 LT in Figure 4.6. From Figure 4.4, the peak value of EEJ on 21st June 2008 which is much higher than any other value is associated with prompt penetration electric field which increases ionization rates. Since CEJ usually results in the reversal of the direction of EEJ, the trough observed on the 21st and 22nd June 2008 as well as on the 21st, 22nd and 23rd September 2008 in Figure 4.5 is associated with CEJ occurrences in these months.

Also noteworthy is the fact that the storm perturbation on EEJ peak on the storm day of March 9th, 2008, was suppressed by the geomagnetic storm ring currents that are flowing westward.

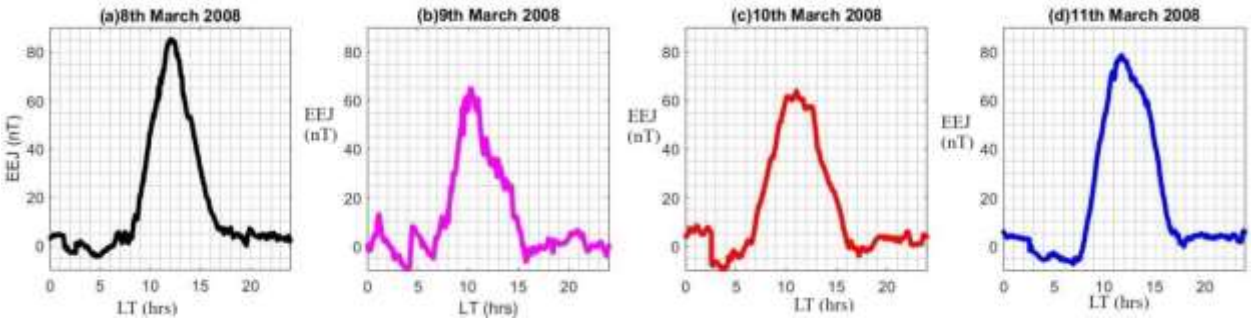

Figure 4.3: The storm perturbation on EEJ against local time during a geomagnetically disturbed day in March 2008

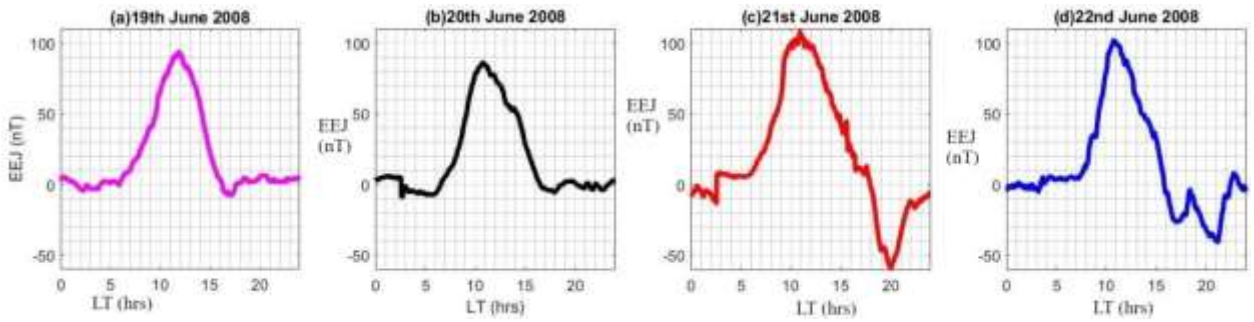

Figure 4.4: The storm perturbation on EEJ against local time during a geomagnetically disturbed day in June 2008

Figure 4.5: The storm perturbation on EEJ against local time during a geomagnetically disturbed day in September 2008

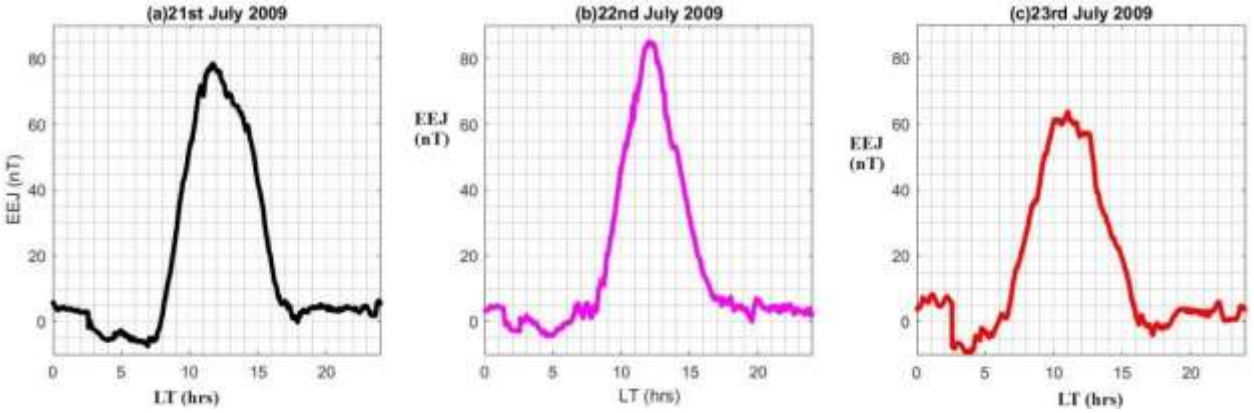

Figure 4.6: The storm perturbation on EEJ against local time during a geomagnetically disturbed day in July 2009

These results are consistent with those obtained by L. Jose, S. Ravindran, C. Vineeth, T. K. Pant and S. Alex (2011) for American, Brazilian and Japanese longitude sectors with the difference in the time of peak associated with the changes in thermospheric wind.

These results for disturbed days clearly show the dependence of the intensity of the storm perturbation on EEJ current on time and seasonal conditions. From Figures 4.3, 4.4, 4.5 and 4.6, there is an increase in the storm perturbation on EEJ peak at the start of the storm due to the sudden commencement of the storm and the presence of a prompt penetration electric field to the equatorial region, increasing ionization rates but later the storm perturbation on EEJ is suppressed. EEJ is later suppressed by the storm due to disturbed dynamo phenomena during storms which reverses zonal electric fields westwards.

The results differ from that of other studies done in Indian and some parts of American regions where the strength of the storm perturbation on EEJ is weaker than in Equatorial regions. This variation is attributed to the change in longitude and latitude which varies from one region to another. For instance, during geomagnetically disturbed days, the cases of EEJ above 50 nT are revealed in 13 panels that are on the 8th, 9th, 10th and 11th March 2008, 19th, 20th, 21st and 22nd June 2008, 21st and 23rd September 2008, 21st, 22nd and 23rd July 2009 with only one panel (22nd September 2008) recording EEJ less than 50nT. See Figure 4.5(b). From the results obtained by other investigators for the American and Indian sectors (Sethia et al., 1980a; Chakraborty & Hajra, 2009b), the EEJ strength is found to vary both monthly following the movement of the electrojet current foci and diurnally following radiation conditions of the sun at that location.

4.2: Quantifying the strength of EIA during the solar minimum period over the East African sector.

4.2.1 The EIA on Geomagnetically Quiet Days

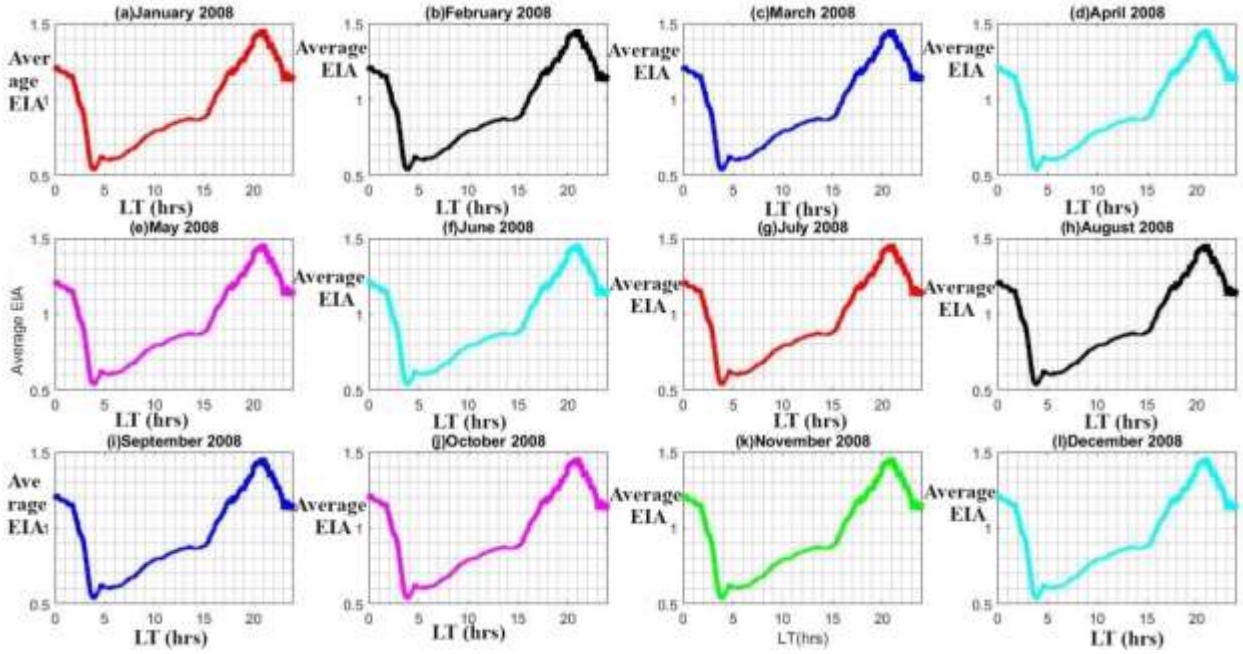

Figure 4.7: Average EIA against Local Time in hours at Mbarara, Uganda in 2008

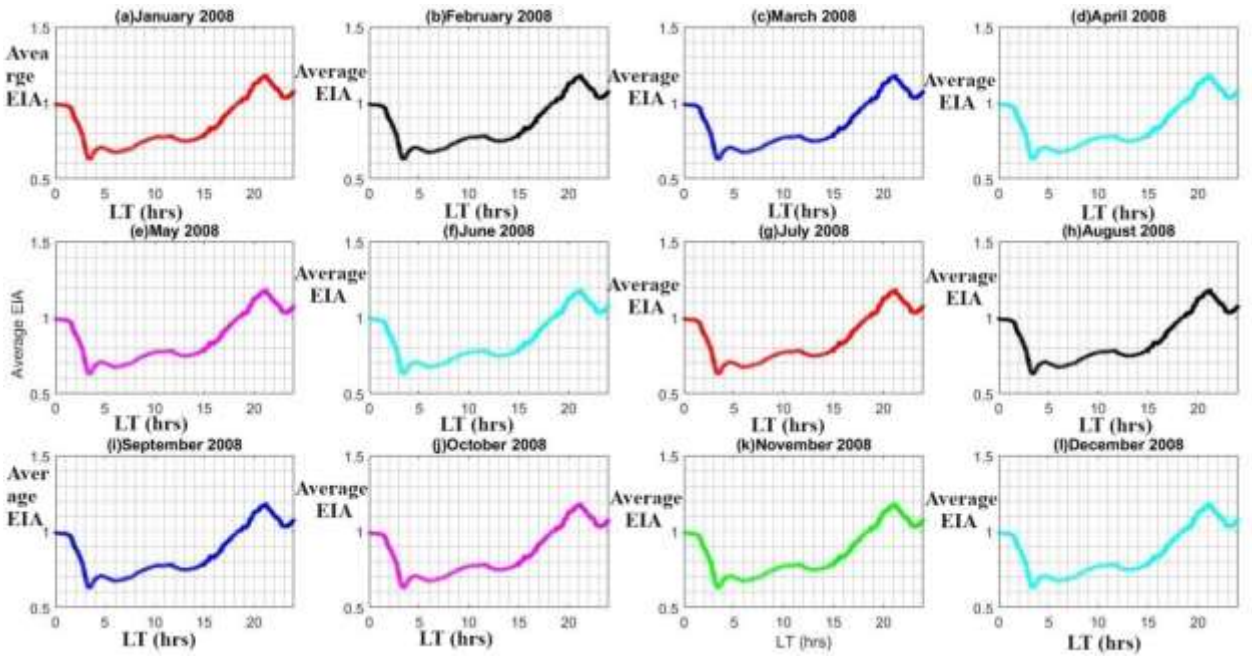

Figure 4.8: Average EIA against Local Time in hours at Nairobi, Kenya in 2008

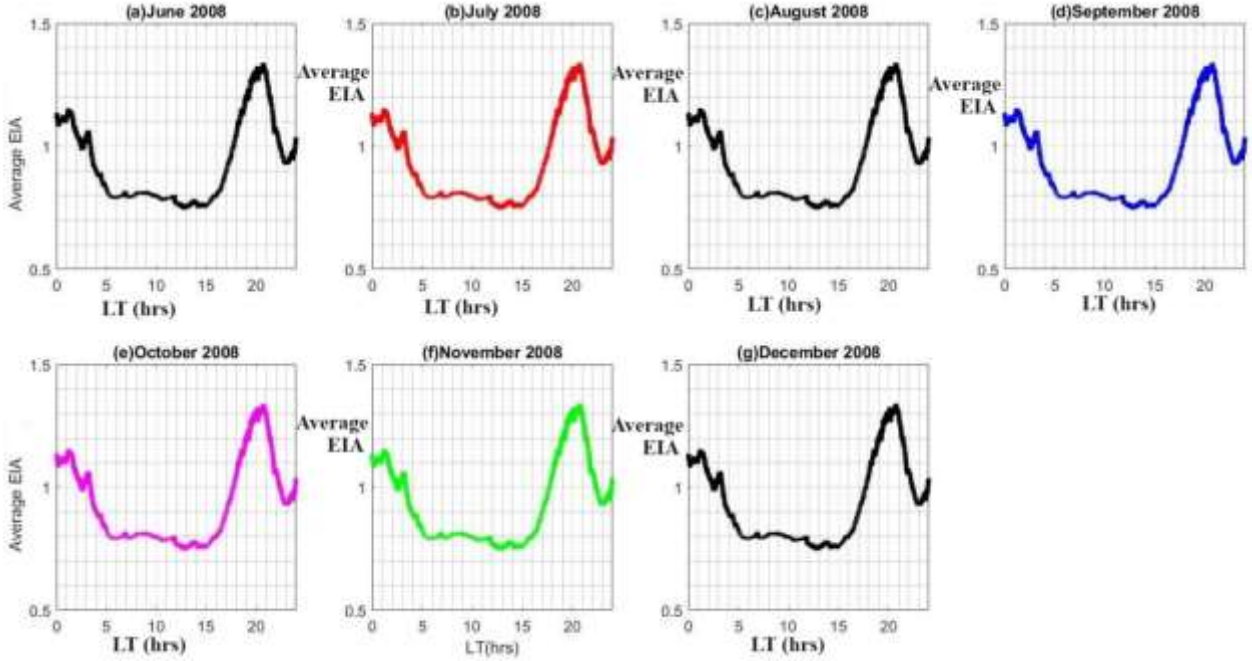

Figure 4.9: Average EIA against Local Time in hours at Malindi, Kenya in 2008

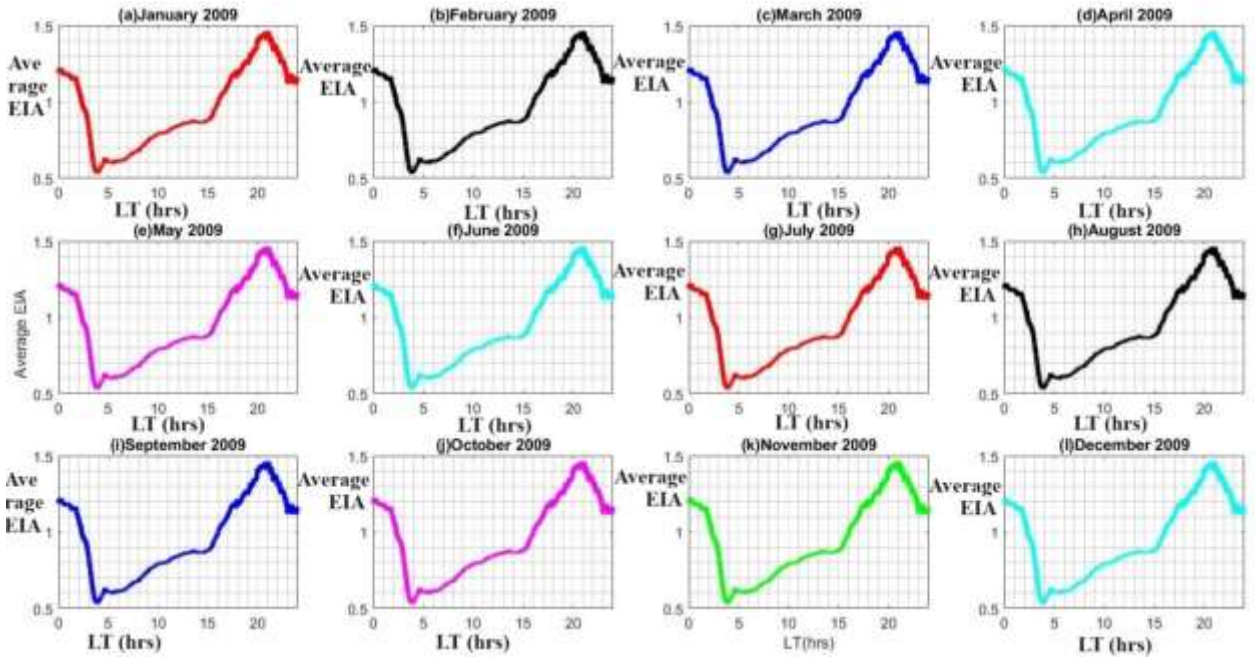

Figure 4.10: Average EIA against Local Time in hours at Mbarara, Uganda in 2009

It is important to note that EIA values greater than 1 were considered as the occurrence of EIA. Therefore, EIA begins building around 09:00 LT and lasts till 20:00 LT in Figures 4.7, 4.8, 4.9 and 4.10. Because the EEJ peaks at noon, cases of substantial EIA 8 hours later are not a result of increasing zonal electric fields associated with higher EEJ. Other circumstances, such as the PRE shortly before this period, could be a contributing cause. There is a clear occurrence of the EIA which exists beyond 20:00 LT, lasting till 24:00 LT in all the months of the year 2008 (see Figures 4.7, 4.8, 4.9 and 4.10). Furthermore, while the fountain effect is primarily responsible for the formation of the EIA, neutral meridional winds at F region altitudes can influence many intricate features of the EIA morphology, according to Sastri (1990). Most of the panels in Figures 4.7, 4.8, 4.9 and 4.10 show that the EIA troughs occur between 03:00 - 04:00 LT and 21:00 – 24:00 LT while the EIA crest occurs at 20:00 LT. The EIA observed between 20:00 and 24:00 LT has a wider trough than that observed between 09:00 and 20:00 LT, owing to the prolonged fountain

effect. The EIA troughs and crests are more prolonged in Mbarara compared to Nairobi and Malindi. In Malindi, the absence of January – May 2008 panels is due to the lack of data for these months across multiple stations. The lack of data would make it more difficult to observe EIA features over the area.

The presence of the EIA over the East African region between 09:00 and 20:00 LT concurs with the findings of Sethia et al., 1980 and Rastogi & Klobuchar, 1990.

4.2.2 The EIA on Geomagnetically disturbed Days

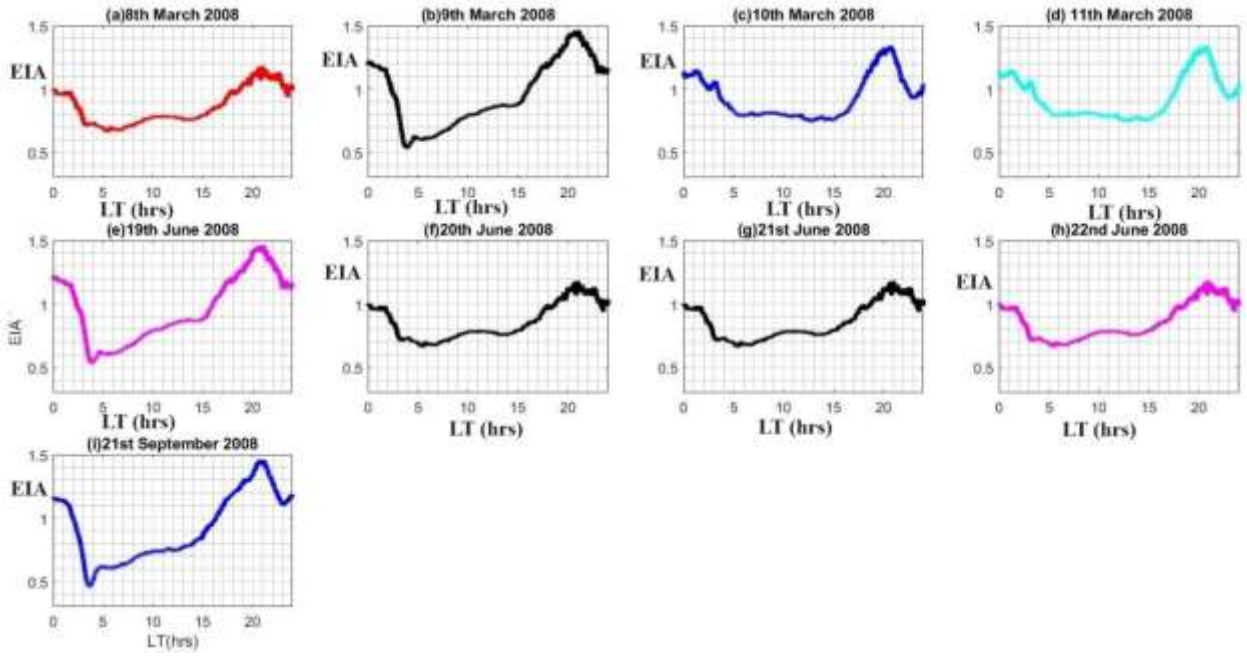

Figure 4.11:EIA against Local Time in hours at Nairobi, Kenya in 2008

Figure 4.12: EIA against Local Time in hours at Nairobi, Kenya in 2009

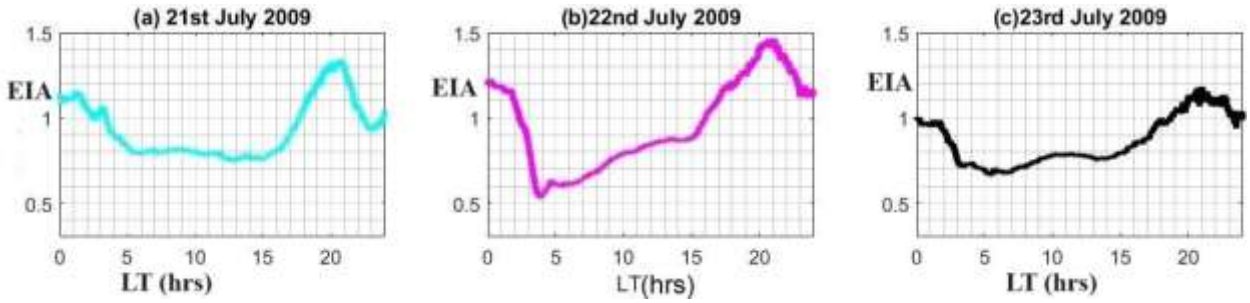

Figure 4.13: EIA against Local Time in hours at Mbarara, Uganda in 2009

The EIA begins building around 04:00 LT and lasts till 20:00 LT in Figures 4.11, 4.12, and 4.13(a) to (l). There is a clear occurrence of the EIA crest in all the geomagnetically disturbed days at 20:00 LT (see Fig. 4.11, 4.12 and 4.13). It can also be observed that all the panels in Figures 4.11, 4.12 and 4.13 show that the EIA troughs occur between 02:00 - 04:00 LT and 22:00 – 24:00 LT. The EIA observed between 02:00 and 04:00 LT has a wider trough while that observed between 22:00 and 24:00 LT has a narrow one. The difference in the extent of the trough observed is due to the prolonged fountain effect. The EIA crests are more prolonged in Mbarara compared to Nairobi and Malindi.

Our results during geomagnetically quiet days differ in some aspects from the study done during geomagnetically quiet days in the low solar activity year of 2009 reported by Bolaji et al. (2017). For instance, their study revealed that the EIA occurrence rarely exceeds 18:00 LT and there was practically no occurrence of the EIA past this time. The highest strength of TEC at the southern crest depicted by their study was about 50 TECU, while our results demonstrated approximately 45 TECU. The increased electron density close to the magnetic equator we observed was due to ionization resulting from the location of the sun above the southern crest close to the zenith. Otherwise, during geomagnetically disturbed conditions, the EIA values increase. This is originated from the increased zonal electric field which results in the increased EIA when plasma

is transported far from the magnetic equator. Another important feature worth mentioning in Figures 4.11, 4.12 and 4.13 is the occurrence of two crests and one trough. Bolaji et al. (2017) also depicted these features over the southern low- and mid-latitude regions of East Africa. However, their emphasis was on the same feature that was observed north of the magnetic equator. They suggested that these scenarios could result from inconsistent transportation of plasma to higher latitudes.

4.3: The correlation between EEJ and EIA.

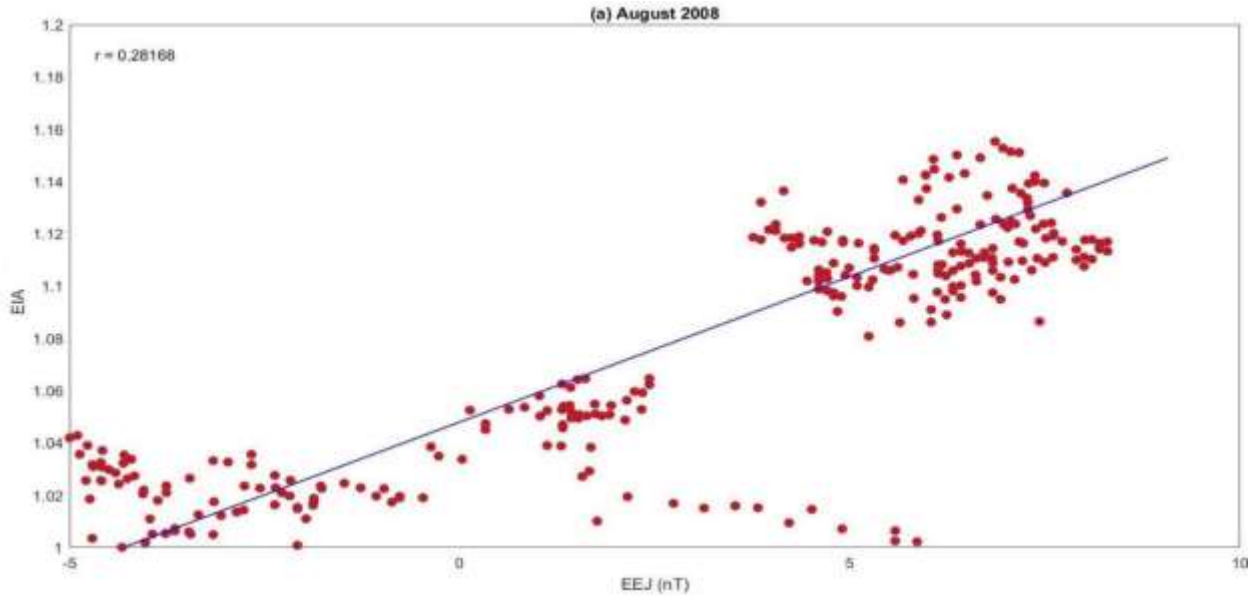

Figure 4.14: EIA against EEJ in Malindi, Kenya during a geomagnetically disturbed day in August 2008.

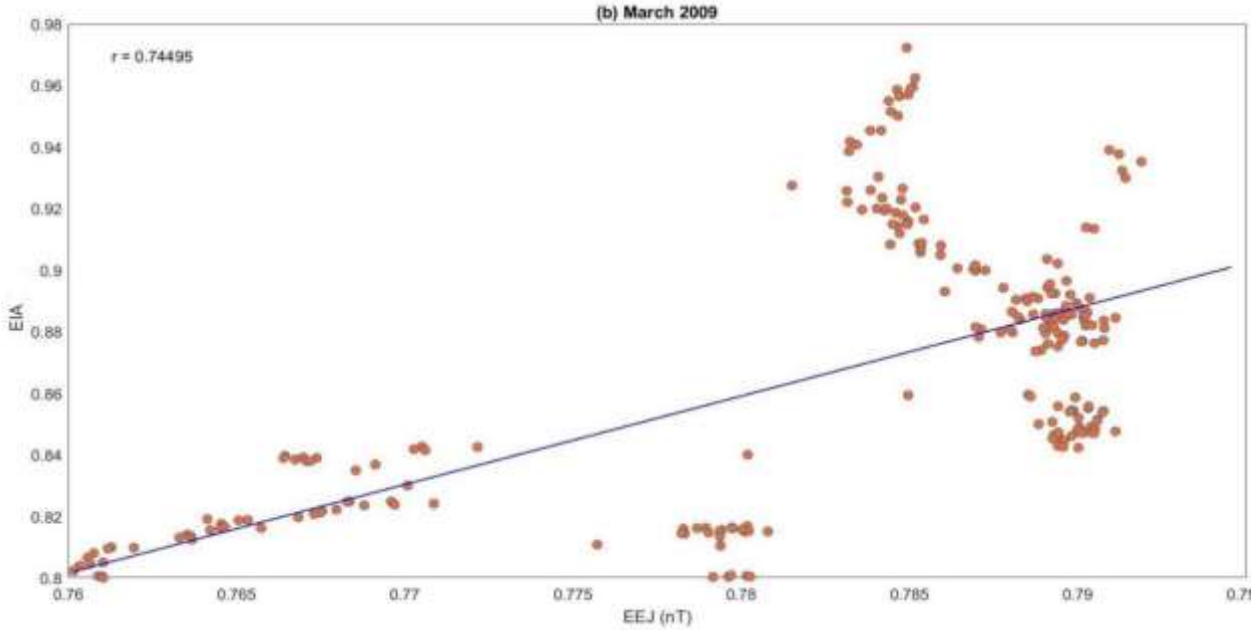

Figure 4.15: EIA against EEJ in Mbarara, Uganda during geomagnetically quiet days in March 2009

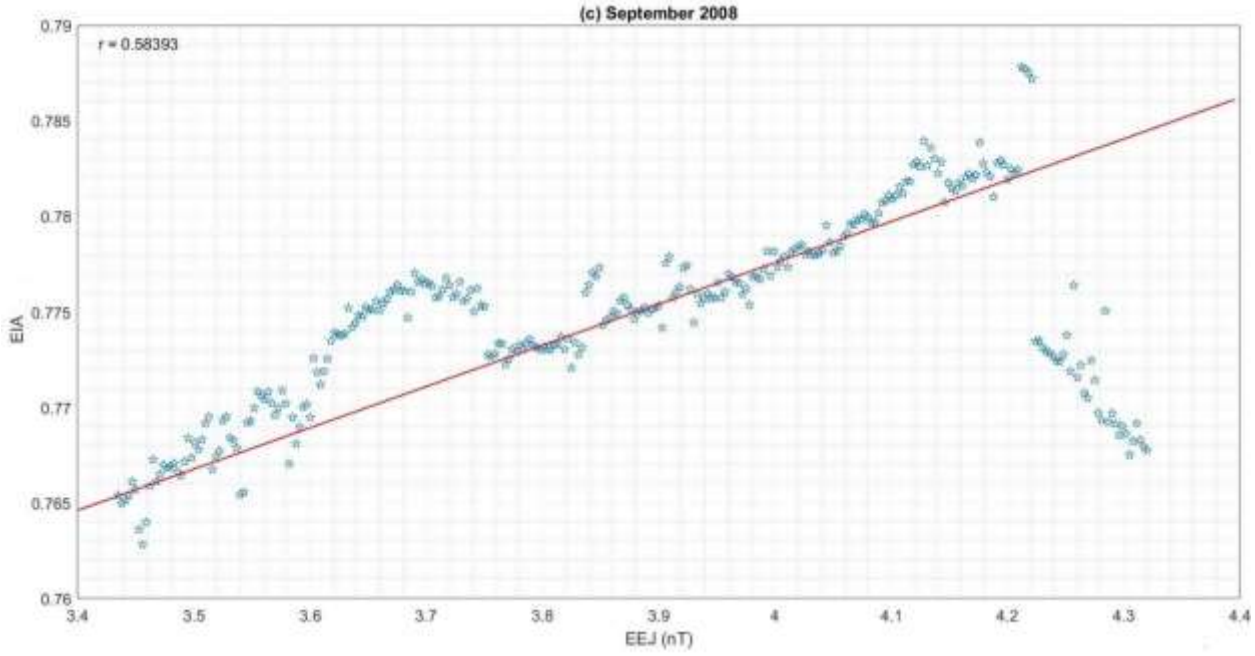

Figure 4.16: EIA against EEJ in Nairobi, Kenya during geomagnetically quiet days in September 2008.

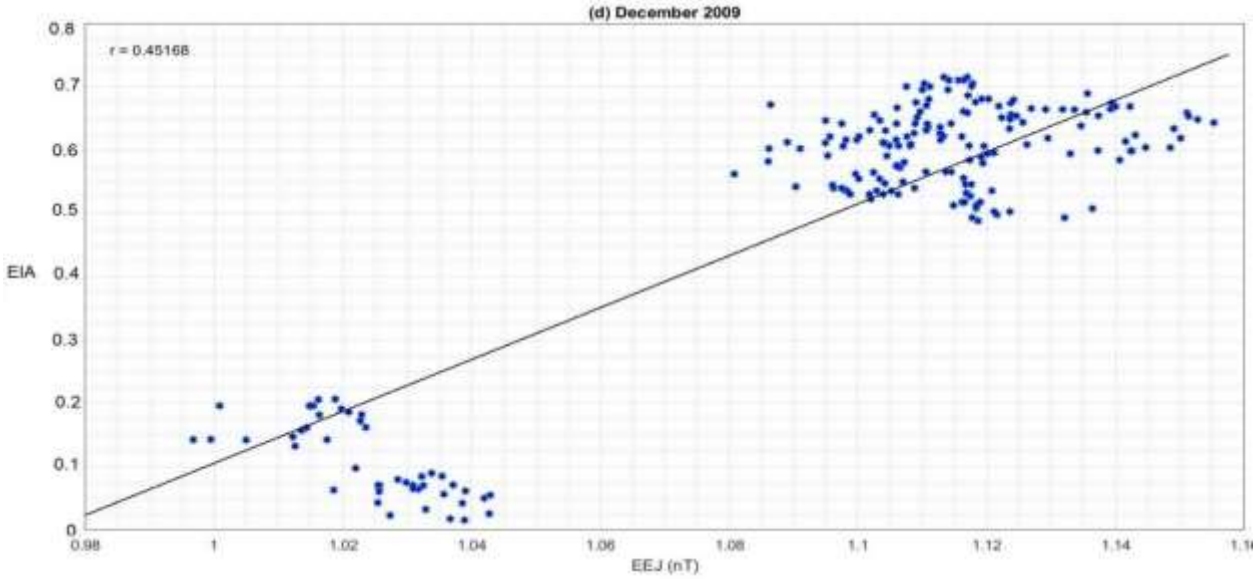

Figure 4.17: EIA against EEJ in Nairobi, Kenya during a geomagnetically disturbed day in December 2009

The scatter plots of EIA against EEJ during both geomagnetically quiet and disturbed conditions are represented in Figures 4.14(Malindi, Kenya), 4.15 (Mbarara, Uganda), 4.16 (Nairobi, Kenya) and 4.17 (Nairobi, Kenya). The correlation analysis was performed on the data corresponding to the years 2008 and 2009, and the coefficients were determined. The EIA was strongly correlated to EEJ in March 2009 in Mbarara, Uganda with a correlation coefficient of 0.74495 (see Figure 4.15) while Figure 4.14 (August 2008 in Malindi, Kenya) shows a weak positive correlation between EIA and EEJ with a correlation coefficient of 0.28168. It is important to note that all the geomagnetically quiet days in August 2008 and December 2009 with Kp $\leq$ 2+ in Malindi and Nairobi respectively were selected. All the days with Kp $\geq$ 5+ were also selected in Mbarara and Nairobi in March 2009 and September 2008. From Figures 4.14, 4.15, 4.16 and 4.17 it can be concluded that the correlation coefficients were found to vary from moderate to strongest during geomagnetically quiet conditions, ranging from 0.58393 to 0.74495. During geomagnetically

disturbed conditions, the correlation coefficient ranges from 0.28168 to 0.45168. (See Figures 4.14, 4.15, 4.16 and 4.17).

The independent increase of the eastward electric field and photo-ionization on TEC is responsible for the strong linear relationship between EEJ and EIA. The strong photoionization during daylight hours results in a higher concentration of free electrons in the equatorial ionosphere contributing to the formation and enhancement of the EIA. Simultaneously, the eastward electric field drives the EEJ near the magnetic equator. The EEJ causes vertical plasma drift in the ionosphere, which redistributes the ionization and electron density. This vertical plasma drift can further enhance the EIA, leading to a strong linear relationship between the strength of the EEJ and the EIA. The TEC is a measure of the integrated electron density along a line of sight through the ionosphere. It is influenced by both the EEJ and the EIA and a strong relationship between these two phenomena can be observed in TEC measurements.

The coefficients thus obtained in the year 2008 are consistent with those obtained using the data corresponding to the year 2009 (EIA and EEJ are strongly correlated during geomagnetically quiet conditions and weakly correlated during disturbed conditions).

CHAPTER FIVE

SUMMARY, CONCLUSION AND RECOMMENDATIONS

The current chapter provides an overview of the thesis main results, explains how the findings can be applied practically and their implications in everyday life, and offers suggestions for further research.

5.1: Summary

The goal of this study was to determine the EEJ strength quantify the strength of the EIA and analyze the correlation between EEJ and EIA during the low solar period from the year (2008) to the year (2009) within the East African region. This was done for both geomagnetically quiet and disturbed conditions. In a nutshell, the following are the main knowledge advancements made by the current study. (a) the peak value of EEJ occurs between 10:00 LT and 14:00 LT which can be attributed to the highest rate of ionization during this period. (b) The highest peak of EEJ occurred in August 2008 recording 110nT and the lowest peak of EEJ (48nT) in September 2008. (c) During the year 2009, the highest peak of 85nT is seen in November 2009 while July 2009 shows the lowest peak (see panels (a) and (d) in Figure 4.2). (d)The results for geomagnetically quiet and disturbed days clearly show the dependence of the intensity of the EEJ current on time and seasonal conditions. The results differ from that of other studies done in Indian and American regions where the strength of the EEJ is weaker during disturbed days than during quiet days. (e) The EEJ strength varies monthly due to the movement of the electrojet current foci and diurnally following radiation conditions of the sun at that location. (f) The EIA appears to begin building around 09:00 LT and last till 20:00 LT. (g) Even though the fountain impact is primarily responsible for the formation of the EIA, neutral meridian winds at altitudes in the F region can have an impact on a variety of subtle aspects of the EIA morphology. (h)The EIA troughs and crests are more prolonged in

Mbarara compared to Nairobi and Malindi. (i) The ratio of crest to trough in most panels is greater than one. (j) The results during geomagnetically disturbed days are different in some ways from the research conducted during geomagnetically quiet days in the relatively low solar activity year of 2009 according to Bolaji et al., 2017. For instance, their research showed that the EIA rarely occurs after 18:00 LT and that there is essentially no EIA activity beyond this hour. (k) Due to ionization caused by the sun's position above the southern crest towards the zenith, a higher electron density was recorded close to the magnetic equator.

5.2: Conclusions

5.2.1: The strength of EEJ

The main results obtained are: (a)The local time of day, season, and solar activity have been found to have an impact on the amplitude of EEJ. The fluctuation in solar heating and ionization rates is what is responsible for this local temporal dependence. (b) It appears that between 11:00 and 13:00 LT, EEJ strength is at its peak. This is due to the high rate of photoionization during this period.

5.2.2: The strength of EIA

The major findings were as follows; (a)The EIA starts accumulating from 9:00 LT and lasts until 20:00 LT. (b) The fountain effect is primarily responsible for the formation of the EIA (c)The EIA troughs and crests are more prolonged in Mbarara compared to Nairobi and Malindi. (d) The maximum EIA strength levels appear to occur between 13:00 and 18:00 LT. As mentioned earlier this is attributed to the prompt penetration electric field which increases ionization rates.

5.2.3: Correlation between EEJ and EIA

The analysis showed that; (a) The correlation coefficients were found to vary from moderate to strongest positive correlation during geomagnetically quiet conditions, ranging from 0.58393 to 0.74495. (b) Geomagnetically disturbed conditions recorded a weak positive correlation with the

correlation coefficient which ranges from 0.28168 to 0.45168. (c) the concurrent rise in photo-ionization and the eastward electric field on TEC is responsible for the strong linear relationship between EEJ and EIA (d) The strongest positive correlation was recorded during geomagnetically quiet days than during geomagnetically disturbed conditions. Similar findings were made by Zhang et al. (2009) and Sethia et al., (1980). They stated that the EIA strength varied semi-annually, with the equinoctial months experiencing the highest peak values.

5.3: Recommendations

5.3.1: To Industry

This research presents patterns in the EEJ and EIA strength over East Africa during the solar minimum period, that can be utilized as a foundation for creating models which can be used to forecast or nowcast scintillations and the ionospheric space weather prediction over this region.

5.3.1: For future or further research

This research presents patterns in the EEJ and EIA strength over East Africa during the solar minimum period. Since EEJ and EIA might influence the occurrence of ionospheric irregularities which in turn lead to scintillations of communication and navigation signals, we recommend simultaneous analysis of EEJ, EIA and scintillation data. This would reveal the influence of EEJ and EIA on the occurrence of scintillations.

REFERENCES

Abadi, P., Saito, S., & Srigutomo, W. (2014). Low-latitude scintillation occurrences around the equatorial anomaly crest over Indonesia. *Annales Geophysicae (09927689), 32*(1).

Amaechi, P. O., Oyeyemi, E. O., & Akala, A. O. (2018). The response of the African equatorial/low-latitude ionosphere to the 2015 St. Patrick's Day geomagnetic storm. *Space Weather, 16*(6), 601–618.

Balan, N., Liu, L., & Le, H. (2018). A brief review of equatorial ionization anomaly and ionospheric irregularities. *Earth and Planetary Physics, 2*(4), 257–275.

Balan, N., Shiokawa, K., Otsuka, Y., Watanabe, S., & Bailey, G. J. (2009). Super plasma fountain and equatorial ionization anomaly during penetration electric field. *Journal of Geophysical Research: Space Physics*, *114*(A3).

Bolaji, O., Owolabi, O., Falayi, E., Jimoh, E., Kotoye, A., Odeyemi, O., Rabiu, B., Doherty, P., Yizengaw, E., & Yamazaki, Y. (2017). Observations of equatorial ionization anomaly over Africa and the Middle East during a year of deep minimum. *Annales Geophysicae*, *35*(1), 123–132.

Campbell, W. H. (2003). *Introduction to geomagnetic fields*. Cambridge University Press.

Chakraborty, S. K., & Hajra, R. (2009a). Electrojet control of ambient ionization near the crest of the equatorial anomaly in the Indien zone. *Annales Geophysicae: Atmospheres, Hydrospheres and Space Sciences*, *27*(1), 93.

Chakraborty, S. K., & Hajra, R. (2009b). Electrojet control of ambient ionization near the crest of the equatorial anomaly in the Indien zone. *Annales Geophysicae: Atmospheres, Hydrospheres and Space Sciences*, *27*(1), 93.

Chen, C.-H., Lin, C.-H., Matsuo, T., & Chen, W. H. (2016). Ionosphere data assimilation modeling of 2015 St. Patrick's Day geomagnetic storm. *Journal of Geophysical Research: Space Physics*, *121*(11), 11–549.

Chen, C.-H., Liu, J.-Y., Yumoto, K., Lin, C.-H., & Fang, T.-W. (2008). Equatorial ionization anomaly of the total electron content and equatorial electrojet of ground-based geomagnetic field strength. *Journal of Atmospheric and Solar-Terrestrial Physics*, *70*(17), 2172–2183.

Eastes, R. W., Solomon, S. C., Daniell, R. E., Anderson, D. N., Burns, A. G., England, S. L., Martinis, C. R., & McClintock, W. E. (2019). Global-scale observations of the equatorial ionization anomaly. *Geophysical Research Letters*, *46*(16), 9318–9326.

Habyarimana, V., Habarulema, J. B., & Mungufeni, P. (2020). On the possible contribution of ionospheric vertical drifts to TEC modelling in low latitudes. *Advances in Space Research*.

Huang, L., Wang, J., Jiang, Y., Huang, J., Chen, Z., & Zhao, K. (2014a). A preliminary study of the single crest phenomenon in total electron content (TEC) in the equatorial anomaly region around 120 E longitude between 1999 and 2012. *Advances in Space Research*, *54*(11), Article 11.

Huang, L., Wang, J., Jiang, Y., Huang, J., Chen, Z., & Zhao, K. (2014b). A preliminary study of the single crest phenomenon in total electron content (TEC) in the equatorial anomaly region around 120 E longitude between 1999 and 2012. *Advances in Space Research*, *54*(11), 2200–2207.

Jose, L., Ravindran, S., Vineeth, C., Pant, T. K., & Alex, S. (2011a). Investigation of the response time of the equatorial ionosphere in the context of the equatorial electrojet and equatorial ionization anomaly. *Annales Geophysicae*, *29*(7), 1267–1275.

Jose, L., Ravindran, S., Vineeth, C., Pant, T. K., & Alex, S. (2011b). Investigation of the response time of the equatorial ionosphere in the context of the equatorial electrojet and equatorial ionization anomaly. *Annales Geophysicae*, *29*(7), 1267–1275.

Joshi, L. M., Sripathi, S., & Singh, R. (2016). Simulation of the low-latitude ionospheric response to 2015 St. Patrick's Day super geomagnetic storm using ionosonde-derived PRE vertical drifts over Indian region. *Journal of Geophysical Research: Space Physics*, *121*(3), Article 3.

Kalita, B. R., Hazarika, R., Kakoti, G., Bhuyan, P. K., Chakrabarty, D., Seemala, G. K., Wang, K., Sharma, S., Yokoyama, T., & Supnithi, P. (2016). Conjugate hemisphere ionospheric response to the St. Patrick's Day storms of 2013 and 2015 in the 100° E longitude sector. *Journal of Geophysical Research: Space Physics*, *121*(11), 11–364.

Lühr, H., Alken, P., & Zhou, Y.-L. (2021). The equatorial electrojet. *Ionosphere Dynamics and Applications*, 281–299.

Mungufeni, P., Habarulema, J. B., Migoya-Orué, Y., & Jurua, E. (2018). Statistical analysis of the correlation between the equatorial electrojet and the occurrence of the equatorial ionization anomaly over the East African sector. *Annales Geophysicae*, *36*(3), 841–853.

Omondi, E. G., Paul, B., & Boniface, N. (2017). Quiet Time Correlation Between Geomagnetic Field Variations and the Dynamics of the East African Equatorial Ionosphere. *International Journal of Astrophysics and Space Science*, *5*(1), Article 1.

Pedatella, N. M., Fuller-Rowell, T., Wang, H., Jin, H., Miyoshi, Y., Fujiwara, H., Shinagawa, H., Liu, H.-L., Sassi, F., & Schmidt, H. (2014). The neutral dynamics during the 2009 sudden stratosphere warming were simulated by different whole atmosphere models. *Journal of Geophysical Research: Space Physics*, *119*(2), 1306–1324.

Rabiu, A. B., Folarin, O. O., Uozumi, T., Abdul Hamid, N. S., & Yoshikawa, A. (2017). Longitudinal variation of equatorial electrojet and the occurrence of its counter electrojet. *Annales Geophysicae*, *35*(3), 535–545.

Raghavarao, R., Sharma, P., & Sivaraman, M. R. (1978). *Correlation of the ionization anomaly with the intensity of the electrojet*.

Rastogi, R. G., & Klobuchar, J. A. (1990). Ionospheric electron content within the equatorial F 2 layer anomaly belt. *Journal of Geophysical Research: Space Physics*, *95*(A11), Article A11.

Rush, C. M., Rush, S. V., Lyons, L. R., & Venkateswaran, S. V. (1969). Equatorial anomaly during a period of declining solar activity. *Radio Science*, *4*(9), 829–841.

Sethia, G., Rastogi, R. G., Deshpande, M. R., & Chandra, H. (1980a). Equatorial electrojet control of the low latitude ionosphere. *Journal of Geomagnetism and Geoelectricity*, *32*(4), 207–216.

Sethia, G., Rastogi, R. G., Deshpande, M. R., & Chandra, H. (1980b). Equatorial electrojet control of the low latitude ionosphere. *Journal of Geomagnetism and Geoelectricity*, *32*(4), Article 4.

Srinivasu, V. K. D., Prasad, D., Niranjan, K., Seemala, G. K., & Venkatesh, K. (2019). L-band scintillation and TEC variations on St. Patrick's Day storm of 17 March 2015 over Indian longitudes using GPS and GLONASS observations. *Journal of Earth System Science*, *128*(3), 69.

Stolle, C., Manoj, C., Lühr, H., Maus, S., & Alken, P. (2008). Estimating the daytime equatorial ionization anomaly strength from electric field proxies. *Journal of Geophysical Research: Space Physics*, *113*(A9).

Venkatesh, K., Fagundes, P. R., Prasad, D. S. V. V. . d., Denardini, C. M., de Abreu, A. J., de Jesus, R., & Gende, M. (2015). Day-to-day variability of equatorial electrojet and its role on the day-to-day characteristics of the equatorial ionization anomaly over the Indian and Brazilian sectors. *Journal of Geophysical Research: Space Physics*, *120*(10), 9117–9131. https://doi.org/10.1002/2015JA021307

Venkatesh, K., Fagundes, P. R., Prasad, D. V., Denardini, C. M., De Abreu, A. J., De Jesus, R., & Gende, M. (2015). Day-to-day variability of equatorial electrojet and its role on the day-to-day characteristics of the equatorial ionization anomaly over the Indian and Brazilian sectors. *Journal of Geophysical Research: Space Physics*, *120*(10), 9117–9131.

Yamazaki, Y., Richmond, A. D., Maute, A., Liu, H.-L., Pedatella, N., & Sassi, F. (2014a). On the day-to-day variation of the equatorial electrojet during quiet periods. *Journal of Geophysical Research: Space Physics*, *119*(8), Article 8.

Yamazaki, Y., Richmond, A. D., Maute, A., Liu, H.-L., Pedatella, N., & Sassi, F. (2014b). On the day-to-day variation of the equatorial electrojet during quiet periods. *Journal of Geophysical Research: Space Physics*, *119*(8), 6966–6980.

Yue, X., Schreiner, W. S., Pedatella, N., Anthes, R. A., Mannucci, A. J., Straus, P. R., & Liu, J.-Y. (2014). Space weather observations by GNSS radio occultation: From FORMOSAT-3/COSMIC to FORMOSAT-7/COSMIC-2. *Space Weather*, *12*(11), Article 11.

APPENDICES

Appendix 1: Determination of EEJ strength script in Matlab

```
clc

clear

% load clc;

% clear

Data=dlmread('E:\Transfered documents\DESKTOP DOCUMENTS\EEJ

2008_2009\disturbed2.txt','\t');%Reading txt file

% Describing data

Time=Data(:,1);

% changeinH=Data(:,11);

% EEJ=Data(:,2);

EEJ=Data(:,2:9);

subplot(1,4,1)

g=plot(Time, EEJ(:,2), 'k', 'LineWidth',3);

ylabel('EEJ (nT)');

% xlabel('UT (hrs)');

box 'on'

axis square;

axis([0 24  -10 90]);

title('(a)8th March 2008');
```

Appendix 2: Determination of EIA strength script in Matlab

```
clc
clear
load DayJAN9;load DayFEB9;load DayMARCH9;load DayAPRIL9;load DayMAY9; load
DayJUNE9;load DayJULY9;load DayAUG9;load DaySEP9;load DayOCT9;load
DayNOV9;load DayDEC9;
subplot(3,4,1), plot(DayJAN9(:,1)/3600, DayJAN9(:,2), 'r', 'LineWidth',3), box on, axis([0 24
0.5 1.5]); title('(a)January 2008 MBAR'); ylabel('Average EIA (nT)'); xlabel('LT(hrs)')
subplot(3,4,2), plot(DayFEB9(:,1)/3600, DayFEB9(:,2), 'k', 'linewidth',3), box on, axis([0 24 0.5
1.5]); title('(b)February 2008');
subplot(3,4,3), plot(DayMARCH9(:,1)/3600, DayMARCH9(:,2), 'b', 'linewidth',3), box on,
axis([0 24 0.5 1.5]); title('(c)March 2008');
subplot(3,4,4), plot(DayAPRIL9(:,1)/3600, DayAPRIL9(:,2), 'c', 'linewidth',3), box on, axis([0
24 0.5 1.5]); title('(d)April 2008');
subplot(3,4,5), plot(DayMAY9(:,1)/3600,DayMAY9(:,2),'m','linewidth',3),box on,axis([0 24 0.5
1.5]); title('(e)May 2008'); ylabel('Average EIA (nT)');
subplot(3,4,6), plot(DayJUNE9(:,1)/3600, DayJUNE9(:,2), 'c', 'linewidth',3), box on, axis([0 24
0.5 1.5]); title('(f)June 2008');
subplot(3,4,7), plot(DayJULY9(:,1)/3600, DayJULY9(:,2), 'r', 'linewidth',3), box on, axis([0 24
0.5 1.5]); title('(g)July 2008');
subplot(3,4,8), plot(DayAUG9(:,1)/3600, DayAUG9(:,2), 'k', 'linewidth',3), box on, axis([0 24
0.5 1.5]); title('(h)August 2008');
```

```
subplot(3,4,9), plot(DaySEP9(:,1)/3600, DaySEP9(:,2), 'b', 'linewidth',3), box on, axis([0 24 0.5
1.5]); title('(i)September 2008');
subplot(3,4,10), plot(DayOCT9(:,1)/3600,DayOCT9(:,2),'m','linewidth',3),box on,axis([0 24 0.5
1.5]); title('(j)October 2008');
subplot(3,4,11), plot(DayNOV9(:,1)/3600, DayNOV9(:,2), 'g',' linewidth',3), box on, axis([0 24
0.5 1.5]); title('(k)November 2008'); xlabel('LT(hrs)')
subplot(3,4,12), plot(DayDEC9(:,1)/3600, DayDEC9(:,2), 'c', 'linewidth',3), box on, axis([0 24
0.5 1.5]); title('(l)December 2008');
```

Appendix 3: Scatter plot script in Matlab

```
clc
clear
Data=dlmread('E:\Transfered documents\DESKTOP DOCUMENTS\EEJ
2008_2009\scatter_Mali2.txt','\t');%Reading txt file
% Describing data
EEJ=Data(:,1);
 Months=Data(:,2:8);
 subplot(2,2,1)
EIA=Data(:,5);
g=scatter(EEJ, EIA,'k', 'DisplayName',' Jan')
xticklabels({'0.78', '0.86', '0.94', '1.00', '1.08', '1.16', '1.24', '1.32', '1.40'})
yticklabels({'0.75', '0.85', '0.95', '1.05', '1.15', '1.25', '1.35'})
ylabel('EIA', 'FontWeight', 'bold'); box 'on';  set(g, 'linewidth',2);  r = corrcoef(EIA, EEJ); str =
['r =',num2str(r(1,2))];  T = text(min(get(gca, 'xlim')), max(get(gca, 'ylim')), str); set(T,
'fontsize', 14, 'verticalalignment', 'top', 'horizontalalignment', 'left');
 hold on
subplot(2,2,2)
EIA=Data(:,4);
g=scatter(EIA,EEJ,'k','DisplayName','Jan'); box 'on';  set(g,'linewidth',2);  r = corrcoef(EIA,
EEJ);  str = ['r =',num2str(r(1,2))]
 T = text(min(get(gca, 'xlim')), max(get(gca, 'ylim')), str);  set(T, 'fontsize', 14,;
'verticalalignment','top','horizontalalignment', 'left');
```

```
 hold on
 subplot(2,2,3)
EIA=Data(:,7); g=scatter(EIA,EEJ,'k','DisplayName','Jan'); box 'on';  set(g,'linewidth',2)
 hold on
xlabel ('EEJ (nT)', 'FontWeight', 'bold');  r = corrcoef(EIA, EEJ);  str = ['r =',num2str(r(1,2))]
 T = text(min(get(gca, 'xlim')), max(get(gca, 'ylim')), str);
 set(T, 'fontsize', 14, 'verticalalignment', 'top', 'horizontalalignment', 'left');
 subplot(2,2,4)
EIA=Data(:,7);
g=scatter(EEJ, EIA,'k', 'DisplayName',' Jan')
box 'on'
 set(g,'linewidth',2)
 hold on
 r = corrcoef(EIA, EEJ)
 str = ['r =',num2str(r(1,2))]
 T = text(min(get(gca, 'xlim')), max(get(gca, 'ylim')), str);
 set(T, 'fontsize', 14, 'verticalalignment', 'top', 'horizontalalignment', 'left');
```